

Exosomes loaded a smart bilayer-hydrogel scaffold with ROS-scavenging and macrophage-reprogramming properties for repairing cartilage defect

Xiaoqing Lu^{a,c,1}, Shimin Dai^{a,1}, Benzhao Huang^a, Shishuo Li^a, Peng Wang^a, Zhibo Zhao^a, Xiao Li^a, Ningbo Li^{b,d}, Jie Wen^b, Yunhan Sun^b, Zhentao Man^{a,c,e,***}, Bing Liu^{b,d,**}, Wei Li^{a,c,*}

^a Department of Joint Surgery, Shandong Provincial Hospital Affiliated to Shandong First Medical University, Jinan, Shandong, 250021, PR China

^b School of Stomatology, Shandong First Medical University & Shandong Academy of Medical Sciences, Jinan, Shandong, 250117, PR China

^c College of Sports Medicine and Rehabilitation, Shandong First Medical University & Shandong Academy of Medical Sciences, Taian, Shandong, 271016, PR China

^d Medical Science and Technology Innovation Center, Shandong First Medical University & Shandong Academy of Medical Sciences, Jinan, Shandong, 250117, PR China

^e Endocrine and Metabolic Diseases Hospital of Shandong First Medical University, Shandong Institute of Endocrine and Metabolic Diseases, Jinan, Shandong, 250062, PR China

ARTICLE INFO

Keywords:

Exosomes
Hydrogels
Cartilage
Reactive oxygen species
Macrophage
Inflammation

ABSTRACT

Enhancing the regeneration of cartilage defects remains challenging owing to limited innate self-healing as well as acute inflammation arising from the overexpression of reactive oxygen species (ROS) in post-traumatic microenvironments. Recently, stem cell-derived exosomes (Exos) have been developed as potential cell-free therapy for cartilage regeneration. Although this approach promotes chondrogenesis, it neglects the emerging inflammatory microenvironment. In this study, a smart bilayer-hydrogel dual-loaded with sodium diclofenac (DC), an anti-inflammatory drug, and Exos from bone marrow-derived mesenchymal stem cells was developed to mitigate initial-stage inflammation and promote late-stage stem-cell recruitment and chondrogenic differentiation. First, the upper-hydrogel composed of phenylboronic-acid-crosslinked polyvinyl alcohol degrades in response to elevated levels of ROS to release DC, which mitigates oxidative stress, thus reprogramming macrophages to the pro-healing state. Subsequently, Exos are slowly released from the lower-hydrogel composed of hyaluronic acid into an optimal microenvironment for the stimulation of chondrogenesis. Both *in vitro* and *in vivo* assays confirmed that the dual-loaded bilayer-hydrogel reduced post-traumatic inflammation and enhanced cartilage regeneration by effectively scavenging ROS and reprogramming macrophages. The proposed platform provides multi-staged therapy, which allows for the optimal harnessing of Exos as a therapeutic for cartilage regeneration.

1. Introduction

Without intervention, articular cartilage (AC) trauma usually leads to post-traumatic osteoarthritis (PTOA), a subtype accounting for 12 % of total osteoarthritis (OA) cases [1]. AC predominantly affects young and active individuals [2]. The common clinical treatment methods for traditional joint cartilage injuries include non steroidal anti-inflammatory drugs (NSAIDs), analgesics, physical therapy, and intra-articular injection [3]. Mainly aimed at alleviating symptoms

related to joint cartilage injury, including pain, inflammation, and functional impairment, but the impact on the intrinsic mechanisms of stimulating cartilage tissue regeneration is often limited [4]. Moreover, the progression of PTOA is considered irreversible. Owing to the avascular nature of cartilage and sparse chondrocytes resident in cartilaginous tissue, damaged cartilage has limited regeneration capability [5,6]. Recruitment of endogenous stem cells from subchondral bone is crucial for *in situ* cartilage regeneration. Recently, exosomes (Exos)-based therapy has been developed as potential acellular therapy for cartilage

Peer review under responsibility of KeAi Communications Co., Ltd.

* Corresponding author.

** Corresponding author.

*** Corresponding author. Department of Joint Surgery, Shandong Provincial Hospital Affiliated to Shandong First Medical University, Jinan, Shandong, 250021, PR China.

E-mail addresses: mztqd1984@163.com (Z. Man), liubing@sdfmu.edu.cn (B. Liu), greatli2000@163.com (W. Li).

¹ These authors contributed equally to this work.

<https://doi.org/10.1016/j.bioactmat.2024.04.017>

Received 4 February 2024; Received in revised form 1 April 2024; Accepted 16 April 2024

2452-199X/© 2024 The Authors. Publishing services by Elsevier B.V. on behalf of KeAi Communications Co. Ltd. This is an open access article under the CC BY-NC-ND license (<http://creativecommons.org/licenses/by-nc-nd/4.0/>).

regeneration to replace stem cell transplantation.

Exosomes (Exos) from bone marrow-derived mesenchymal stem cells (BMSCs) can recapitulate the effect of native cells on cartilage defects without the associated side effects of stem cells [7,8]. Abundant miR-23a-3p within Exos inhibits phosphatase and tensin homolog (PTEN) levels and enhances protein kinase B (AKT) expression, thus promoting cartilage regeneration [9,10]. Moreover, Exos recruit BMSCs and promote neo-cartilage formation via the chemokine signaling pathway [11]. In recent years, there have been numerous studies on Exos as a therapeutic agent and as an integrated component of a delivery biomaterial for cartilage repair, providing encouraging results [12]. In particular, Exos internalized by endogenous chondrocytes and BMSCs have been shown to enhance cell migration, proliferation, and chondrogenic differentiation [13]. Trauma to articular cartilage, especially when it develops to PTOA, is commonly associated with excessive inflammation [14]. However, current approaches using Exos for cartilage repair pay close attention to the cartilage regeneration phase, with limited attention to the preceding inflammatory stage [15,16]. Although BMSC-derived Exos exhibit immunomodulation in some cases, the molecular cargo and structure of Exos may be subject to interference arising from the oxidative stress conditions, thereby possibly limiting or diluting the tissue regeneration effect [17]. Therefore, under these conditions, induction of the chondrogenic differentiation of endogenous stem cells would also be suppressed [18]. Consequently, to more fully utilize Exos as a cell-free therapeutic drug for cartilage regeneration during cell proliferation, precisely regulating the emerging inflammatory microenvironment is a critical factor [19].

The chronic inflammatory microenvironment resulting from AC damage is inundated with various activated inflammatory cells and pro-inflammatory mediators, along with reactive oxygen species (ROS) [20, 21]. During cartilage injury, overexpressed ROS not only attacks the extracellular matrix (ECM) of the AC directly but also induces lipid peroxidation and DNA cleavage, which destabilizes the microenvironment [22]. Furthermore, ROS overexpression at cartilage defect sites exacerbates inflammation, thereby creating an intense pro-inflammatory microenvironment, which may compromise downstream cellular functions and lead to impaired healing [23]. ROS-responsive and scavenging biomaterials are smart materials that can directly mitigate oxidative stress in the inflammatory microenvironment. These biomaterials offer the distinct advantage of promptly and effectively eliminating ROS while also serving as carriers for the controlled release of therapeutics in response to elevated levels of ROS [24]. Recent investigations have shown that combined ROS-elimination treatment and anti-inflammatory drugs can synergistically decelerate the progression of inflammation more effectively than either treatment in isolation [25,26]. Sodium diclofenac (DC) is a non-steroidal anti-inflammatory drug that inhibits prostaglandin synthesis through the blockade of cyclooxygenase 1 (COX-1) and cyclooxygenase 2 (COX-2) to reduce pain and inflammation at the site of injury [27]. Sodium diclofenac mainly indirectly affects macrophage polarization by regulating the inflammatory environment. This process mainly involves inhibiting lipoxygenase and inhibiting NF- κ B signal pathway is used to suppress M1 polarization [19]. And it can induce the expression of anti-inflammatory cytokines, such as interleukin (IL-10), and regulate the production of ROS. These environmental improvements can all affect the transformation of macrophages into M2 type status [28]. Therefore, DC release from ROS-responsive and scavenging biomaterials prior to Exos release into the cartilage defect site may afford a greenhouse for Exos to regulate immune responses and promote cartilage regeneration.

Herein, we developed an ROS-responsive bilayer-hydrogel loaded with Exos (Bil-Gel_{DC/Exos}) to link the inflammatory stage with the proliferation stage (Fig. 1). This design aims to alleviate the detrimental effects of the inflammatory environment on BMSCs differentiation and chondrocyte function by linking the two stages. It seeks to enhance the therapeutic efficiency of Exos in the application of cartilage repair,

addressing the limitations of approaches that solely focus on a single stage. Specifically, a hyaluronic acid (HA)-based hydrogel encapsulating Exos was selected as the lower-hydrogel (Low-Gel_{Exos}). HA is the main component of articular cartilage and synovial fluid, which plays a crucial role in the joint lubrication and cartilage tissue protection via recognizing HA receptors (differentiation group 44, CD44). As the main component of the lower-hydrogel, it mimicked the ECM of cartilage and facilitated the effective fusion of the newborn cartilage with the surrounding cartilage [29]. A polyvinyl alcohol (PVA)-based hydrogel loaded with DC was designed as the upper-hydrogel (Up-Gel_{DC}) to create an anti-inflammatory microenvironment by degrading in response to elevated levels of ROS and then releasing DC. The phenylboronic acid in the upper-hydrogel could form reversible bonds with the *cis*-diol groups contained in the abundant glycosaminoglycans in cartilage tissue, conducting to the integration between the hydrogel and cartilage. In addition, the two layers of the hydrogel systems were bound together by the ways of hydrogen bonding, boric acid bonding and electrostatic interaction. Therefore the whole bilayer-hydrogel scaffold was expected to perform mechanical stability during implantation [30]. The performance of this bilayer-hydrogel in reducing oxidative stress and promoting cartilage repair was evaluated through *in vitro* and *in vivo* experiments. With the improved immunological microenvironment by the upper-hydrogel, the sustained release of Exos from the lower-hydrogel over several days enhanced cell-cell interactions and promoted chondrogenic repair. Benefiting from the bilayer structure, Exos functioned optimally and facilitated cartilage repair and regeneration under a favorable “umbrella” environment created by the upper-hydrogel.

2. Materials and methods

2.1. Construction of the bilayer-hydrogel

2.1.1. Preparation of the upper-hydrogel

4-(Bromomethyl) phenylboronic acid (4-BPBA, 1.0 g) and *N, N, N', N'*-tetramethyl-1,3-propanediamine (TMPDA, 0.2 g) were added to dimethylformamide (DMF, 40 mL). The solution was stirred at 60 °C for 24 h and then poured into tetrahydrofuran (THF, 100 mL). It was then filtered, and the residue was washed with THF three times [31]. After drying under vacuum, *N*¹-(4-boronobenzyl)-*N*³-(4-boronophenyl)-*N*¹, *N*¹, *N*³, *N*³-tetramethyl-1,3-propanediaminium (TSPBA) was obtained with a yield of 69.76 % (0.59 g). PVA (5 g) was completely dissolved in deionized water (100 mL) with stirring at 90 °C. TSPBA (5 wt% in H₂O, 1 mL) was mixed with PVA (5 wt%, 2 mL) to form a ROS-responsive hydrogel. Finally, a predetermined amount of DC was added to the TSPBA solution to obtain the upper-hydrogel.

2.1.2. Preparation of the lower-hydrogel

Hydrogel performance is influenced by various factors, including the elastic modulus, porosity, and swelling ratio. To optimize the hydrogel for loading Exos, we prepared hydrogels with different HA contents. In brief, sodium alginate (SA, 1.0 g, 2 wt%) and HA (0.25 g, 0.5 g, 1.0 g) were dissolved in 50 mL of deionized water at 40 °C (water bath), resulting in three gelatinous solutions with different HA/SA ratios (1:4, 1:2, 1:1 w/w). After cooling, Exos were incorporated into the mixture, which was then placed in a mold. Spraying calcium ions (calcium chloride solution, 100 mM) evenly on the surface of the mold using a spray can. When the calcium ions were fully penetrated, the SA macromolecular chain was successfully cross-linked, while encapsulating the free HA macromolecules.

2.1.3. Preparation of the bilayer-hydrogel

First, the lower-hydrogel was prepared in a mold. Next, a PVA solution was added, to which a TSPBA solution containing sodium diclofenac was thoroughly mixed. The upper and lower hydrogels with the proportion of 1:1 was subjected to freezing and thawing repeatedly to

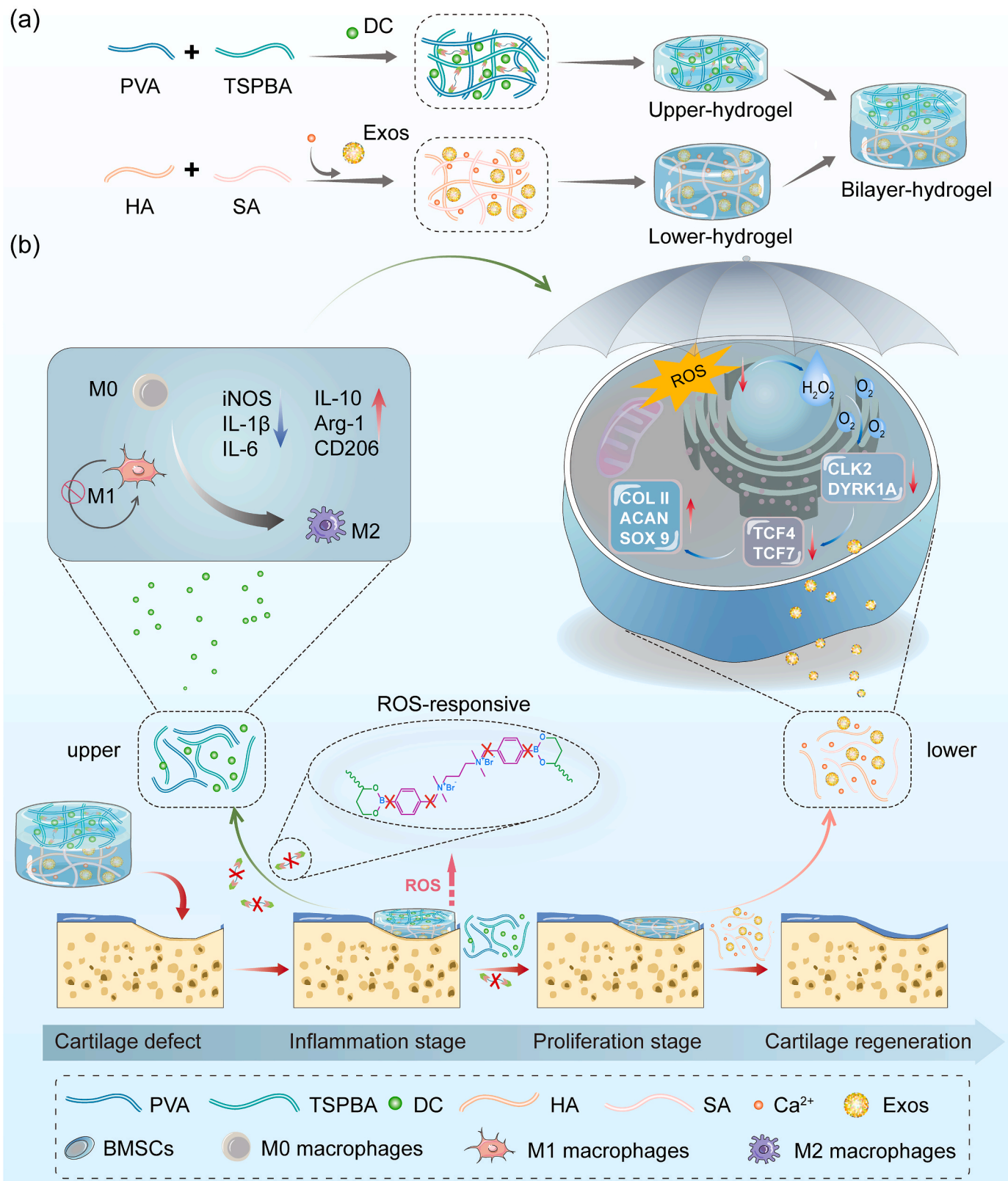


Fig. 1. Schematic illustration of the fabrication of bilayer-hydrogel and the successive promotion of multiple cartilage regeneration phases by bilayer-hydrogel. (a) Preparation of bilayer-hydrogel. (b) An increase in the ROS level at the cartilage injury site triggers the degradation of the upper-hydrogel and the release of DC for inflammation regulation. Subsequently, the lower-hydrogel slowly released Exos in the suitable microenvironment provided by the upper-hydrogel to repair cartilage damage.

obtain a stable structure. After that, the two layers were well bonded due to multiple bond interactions at the interface between the upper and lower hydrogel [32].

2.2. Material characterization

2.2.1. Surface morphology

The surface morphologies of the hydrogels were determined using scanning electron microscopy (SEM, SU-8010, Japan) equipped with an energy dispersive spectroscopy (EDS). Samples were freeze-dried, and the cross-sections of the samples were coated with a gold layer to enhance the conductivity for SEM. The porous structures of the hydrogels were examined, and the pore size was quantified using ImageJ.

2.2.2. Mechanical properties

The rheological properties of the hydrogels (lower-hydrogel with different HA/SA ratios, upper-hydrogel containing DC, and upper-hydrogel without DC) were determined using a rheometer (MCR301, Austria) equipped with 25 mm parallel plates. Experiments were conducted at 25 °C, and the energy storage modulus (G') and loss modulus (G'') were recorded.

2.2.3. Physical properties

The swelling behavior of the lower-hydrogel in water was determined as follows. Freeze-dried hydrogel samples (W_0) were weighed and then immersed in distilled water at room temperature for 20 s. Samples were periodically removed from water, gently blotted with absorbent paper until no more water dripped, and then weighed again (W_t). The swelling ratio (SR) of the hydrogel was calculated using the following equation: $SR = (W_t - W_0) / W_0 \times 100\%$ [33].

To study the degradation behavior of the upper and lower hydrogels under the same conditions, 1 ml of the bilayer-hydrogel consisting of Up-Gel_{DC} and Low-Gel_{Exos} was immersed in 10 mL of simulated body fluid (SBF) containing 10 mM H₂O₂ and incubated at 37 °C. At a preset time point, the Up-Gel_{DC} and Low-Gel_{Exos} were separated and weighed.

2.2.4. Release of Exos and DC from hydrogels

Equal volumes of Up-Gel_{DC} and Low-Gel_{Exos} were used to form a 200 μ L bilayer-hydrogel, which was then immersed in 2 mL of phosphate-buffered saline (PBS) containing 10 mM H₂O₂ and incubated at 37 °C to investigate the release kinetics of DC and Exos from the bilayer-hydrogel. Supernatant (200 μ L) was collected from the tube at specified time intervals, and an equal volume of fresh PBS was replenished. The concentration of Exos in the supernatant was determined by measuring the OD at 265 nm using a UV spectrophotometer (MIULAB, China) and employing a bicinchoninic acid (BCA) protein assay kit (Beyotime, China) to quantify the protein content. Finally, the cumulative release of DC and Exos from the bilayer-hydrogel was calculated.

2.3. Evaluation of H₂O₂-scavenging ability

H₂O₂ oxidizes and hydrolyzes TSPBA, which degrades the upper-hydrogel scaffold to release the payload, DC. To observe its morphology change over time, the upper-hydrogel was immersed in PBS containing 10 mM H₂O₂ at 37 °C. Additionally, the H₂O₂ concentration was determined using the titanium sulfate colorimetric method (hydrogen peroxide detection kit, LEAGENE, China).

2.4. Uptake of Exos

The phagocytosis of Exos encapsulated in the lower-hydrogel by BMSCs was investigated as follows. We first performed Exos isolation, identification and staining. Exos were initially labeled with PKH 26 and subsequently co-incubated with BMSCs for 24 h. The cells were then fixed at room temperature and stained with TRITC-phalloidin (Invitrogen, USA) and 4-6-diamidino-2-phenylindole (DAPI, Invitrogen) to

identify the cytoskeleton and nucleus, respectively. Finally, labeled cells were observed using a confocal microscope (EVOS™ M7000, USA).

2.5. In vitro biocompatibility assessment

The cytocompatibility of the hydrogels were evaluated using a live/dead staining kit (Invitrogen) and CCK-8 assay kit (Beyotime). For live/dead staining, BMSCs were cultured with the lower-hydrogels (three different HA/SA ratios) for 1, 2, and 3 days. Staining was conducted per manufacturer's instructions, and the cells were observed using a confocal microscope (EVOS™ M7000). Three randomly selected fields-of-view were used to quantify cell viability with ImageJ. For the cytotoxicity assay, BMSCs were co-cultured with extracts of the lower-hydrogels (three different HA/SA ratios) for 1, 2, and 3 days. Subsequently, 100 μ L of CCK-8 solution (100 μ L/mL) was added to each well, and incubation continued for 2 h. A microplate reader (Tecan Spark, Switzerland) was used to measure the absorbance of cells in each well at 450 nm.

Similarly, the upper-hydrogel (loaded with DC) was co-cultured with RAW264.7 for the above viability and proliferation assays.

2.6. Validation of ROS-scavenging

The ROS clearance ability of the upper-hydrogel was validated as follows. RAW264.7 cells were co-cultured with Up-Gel and Up-Gel_{DC} for 24 h and then exposed to H₂O₂ (100 μ M) for 3 h. The control group was untreated. Subsequently, the cells were stained with DCFH-DA (10 μ M, Sigma-Aldrich, China) for 30 min and observed using a confocal microscope. Following the similar procedure, cells were collected in flow tubes after DCFH-DA staining. The intracellular ROS levels were measured using a flow cytometer (Cytek Aurora, USA) and data analysis was performed using FlowJo.

2.7. Flow cytometry analysis of macrophage polarization

RAW264.7 cells were co-cultured with the upper-hydrogel in well plates and stimulated with either LPS (100 ng/mL) or IL-4 (20 ng/mL). Afterwards, the cells were washed with pre-cooled PBS to prepare single-cell suspensions. This was followed by a series of steps, including fixation, membrane-breaking, and incubation with antibodies targeting M1 marker CD86 and M2 marker CD206 (Thermo Fisher Scientific). Subsequently, the cells were analyzed using a flow cytometer and analyzed using FlowJo.

2.8. Validation of chondrocyte protection

To confirm the chondroprotection effect of the bilayer-hydrogel, we used JC-1 to measure the mitochondrial membrane potential and TUNEL staining to detect nuclear DNA breakage during the apoptosis of cells. Early apoptosis was assessed using the mitochondrial membrane potential detection kit (JC-1, Beyotime). Per manufacturer's instructions, cells in 24-well plates were stained with JC-1 staining solution at 37 °C for 20 min. Then, each well was washed twice with 1 \times JC-1 staining buffer, and the fluorescence intensity was measured using a confocal microscope. The red-to-green fluorescence ratio reflects changes in the mitochondrial membrane potential. To investigate chondrocyte apoptosis, cells were stained with a one-step TUNEL apoptosis assay kit (Elabscience, China) per manufacturer's instructions and observed under a confocal microscope (EVOS™ M7000).

2.9. Gene expression

Total cellular RNA was determined using an RNA extraction kit (Omega, USA). cDNA synthesis was performed using a PrimeScript RT reagent kit (Takara, Japan), and qPCR amplification was conducted using the qPCR SYBR green master mix (Yeasen, China). The GAPDH

gene was used as an internal control. Relative gene expression levels were measured using the $2^{-\Delta\Delta Ct}$ method. The expressions of inflammation-related genes (*IL-1 β* , *IL-6*, *iNOS*, *IL-10*, *Arg-1*, *CD206*), chondrocyte differentiation-related genes (*COL II*, *Sox9*, *ACAN*) and pathway-related genes (*CLK2*, *DYRK1A*, *TCF4*, *TCF7*) were evaluated. The experiments of real-time quantitative PCR (qPCR) were repeated three times independently. Primers for this study were purchased from Tsingke Biotech (China), and the sequences are listed in Table S1.

2.10. Immunofluorescence

For immunofluorescence staining, the medium was removed and fixed for 30 min with 4 % PFA. Then, samples were treated with 0.3 % Triton X-100 (Biofroxx, Germany) for 10 min and blocked with 5 % goat serum (Beyotime) for 1 h. Samples were incubated with primary antibodies overnight at 4 °C. Subsequently, secondary antibodies were applied, followed by nuclear staining with DAPI for 5 min. Finally, fluorescence images were taken using a widefield fluorescence imaging system (Zeiss celldiscoverer 7, Germany). The antibodies used are listed in Table S2.

2.11. Western blotting

The cells were collected and added to RIPA lysis buffer (Beyotime) containing protease and phosphatase inhibitors (Sigma–Aldrich). Then, the solution was centrifuged at 12000 rpm for 30 min at 4 °C to isolate the supernatant. SDS-PAGE was used to separate the proteins, which were transferred onto 0.45 μ m PVDF membrane (Millipore, USA), blocked with QuickBlock™ blocking buffer (Beyotime), and then incubated with primary antibodies (listed in Table S2) at 4 °C overnight. Finally, the proteins were incubated with secondary antibodies (Proteintech, China) at room temperature for 2 h. An enhanced chemiluminescence kit (Millipore) was applied to detect the proteins, which were quantified using ImageJ.

2.12. RNA sequencing and bioinformatics

RAW264.7 cells were cultured with the bilayer-hydrogel for 3 days, and the supernatant was collected after centrifugation. BMSCs were incubated with differentiation medium (supernatant: basic differentiation medium = 1:1) for 7 days. The basic differentiation medium contained Dulbecco's Modified Eagle Medium (DMEM), 10 % fetal bovine serum (FBS), 1 % penicillin/streptomycin, 0.05 % 100 \times ITS, 50 μ M ascorbic acid, and 100 nM dexamethasone. After 7 days of culturing, samples were collected and treated with Trizol reagent (Beyotime) and stored at –80 °C for sequencing [34]. Extracted total RNA was sent to Oebiotech (China) for library preparation, RNA sequencing (RNA-seq), and data analysis.

2.13. In vivo ROS-scavenging assessment and rat cartilage defect model

All procedures adhered to the National Institutes of Health (NIH) Guide for the Care and Use of Laboratory Animals, and received approval from the Animal Ethics Committee of Shandong Provincial Hospital Affiliated to Shandong First Medical University (No. 2023-013). In this study, 33 Sprague–Dawley (SD) rats (male, 300 g) were used. The immunomodulatory and cartilage repair effects of Bil-Gel_{DC}/Exos *in vivo* were evaluated using subcutaneous implantation and cartilage defect models. To create the subcutaneous implantation model, we shaved and sterilized the dorsal surgical site of 9 SD rats and made two incisions to create subcutaneous pockets. Two hydrogels were implanted in each rat, and the wounds were sutured. Three rats were injected with ROS-specific chemiluminescence probe L-012 (Sigma–Aldrich) to evaluate the ROS clearance ability *in vivo*. Chemiluminescence images were observed using an *in vivo* imaging system (IVIS Lumina K Series III, PerkinElmer, USA). Six rats were euthanized directly, and tissue samples

were collected to evaluate immune regulation effects [24]. The cartilage defect model was established by using a drill bit to create full-thickness cylindrical cartilage defects (2.0 mm in diameter, 1 mm in depth) on the distal femoral trochlear groove of 24 SD rats. The choice of left or right legs for surgery was randomized to minimize individual differences. The rats were randomly divided into four groups: 1) Control; 2) Up-Gel_{DC}; 3) Low-Gel_{Exos}; 4) Bil-Gel_{DC}/Exos. At 4 and 8 weeks postoperative, the rats were euthanized using carbon dioxide, and tissue samples were collected.

2.14. Macroscopic assessment and MRI

At 4 and 8 weeks post-surgery, cartilage repair was macroscopically evaluated using the criteria of the International Cartilage Repair Society (ICRS). Specifically, defect filling, tissue integration, and surface smoothness were assessed through visual inspection of each knee joint. Magnetic resonance imaging (MRI; Siemens, Germany) was used to confirm new cartilage growth.

2.15. Histological evaluation

Tissue samples from rats with subcutaneous implants were histologically analyzed using hematoxylin and eosin (H&E), macrophage markers (iNOS marker M1, CD206 marker M2) for immunofluorescence. Knee tissue samples were collected for histological analysis of cartilage repair at 4 and 8 weeks postoperation using H&E, safranin O/fast green (SOFG), toluidine blue (TB), immunochemistry, and immunofluorescence.

2.16. Statistical analysis

All data are expressed as the mean \pm standard deviation ($n \geq 3$). Variations between multiple groups were assessed using one-way analysis of variance (ANOVA). Results were analyzed and compared using GraphPad Prism software (La Jolla, CA). Statistical significance was set as ns = not significant, * $p < 0.05$, ** $p < 0.01$, *** $p < 0.001$.

3. Results

3.1. Synthesis, characterization, and ROS-scavenging ability of the upper-hydrogel

The ROS-responsive upper-hydrogel was obtained by crosslinking PVA with ROS-responsive linker TSPBA. SEM revealed that the upper-hydrogel had a porous network structure (Fig. 2A). TSPBA was synthesized through the quaternization of TMPDA with excess 4-BPBA and was evaluated with ¹H NMR (Fig. 2B). The formation of the upper-hydrogel was due to the fact that TSPBA contains two phenylboronic acids, which complexed with the diol on the PVA (Fig. S1A and B). Through live/dead staining and CCK-8 experiments, we selected 2 μ g/mL as the optimal concentration for loading DC onto the upper-hydrogel (Fig. S2). We assessed the upper-hydrogel ability of ROS-scavenging using a titanium sulfate oxidation assay kit. Within 60 h, it was able to eliminate 10 mM H₂O₂ and completely release the loaded DC (Fig. 2C and D). Through degradation experiments (Figs. S3A and B), we visually observed the changes of the upper-hydrogel in H₂O₂, and the degradation rate was directly proportional to the ROS levels. As the H₂O₂ concentration increased, the volume of the hydrogel decreased. This response characteristic allowed for the release of drugs in varying amounts based on the degree of inflammation. Meanwhile, the upper-hydrogel exhibited solid like viscoelasticity with higher storage modulus (G') and lower loss modulus (G'') as shown in the rheological experiments (Fig. 2E), indicating the successful gelation of PVA and TSPBA. The modulus of the hydrogel was hardly affected after DC loading. As shown in Fig. 2F, the upper-hydrogel exhibited strong adhesiveness, capable of adhering to different substances, which provided the basis for a good bonding with

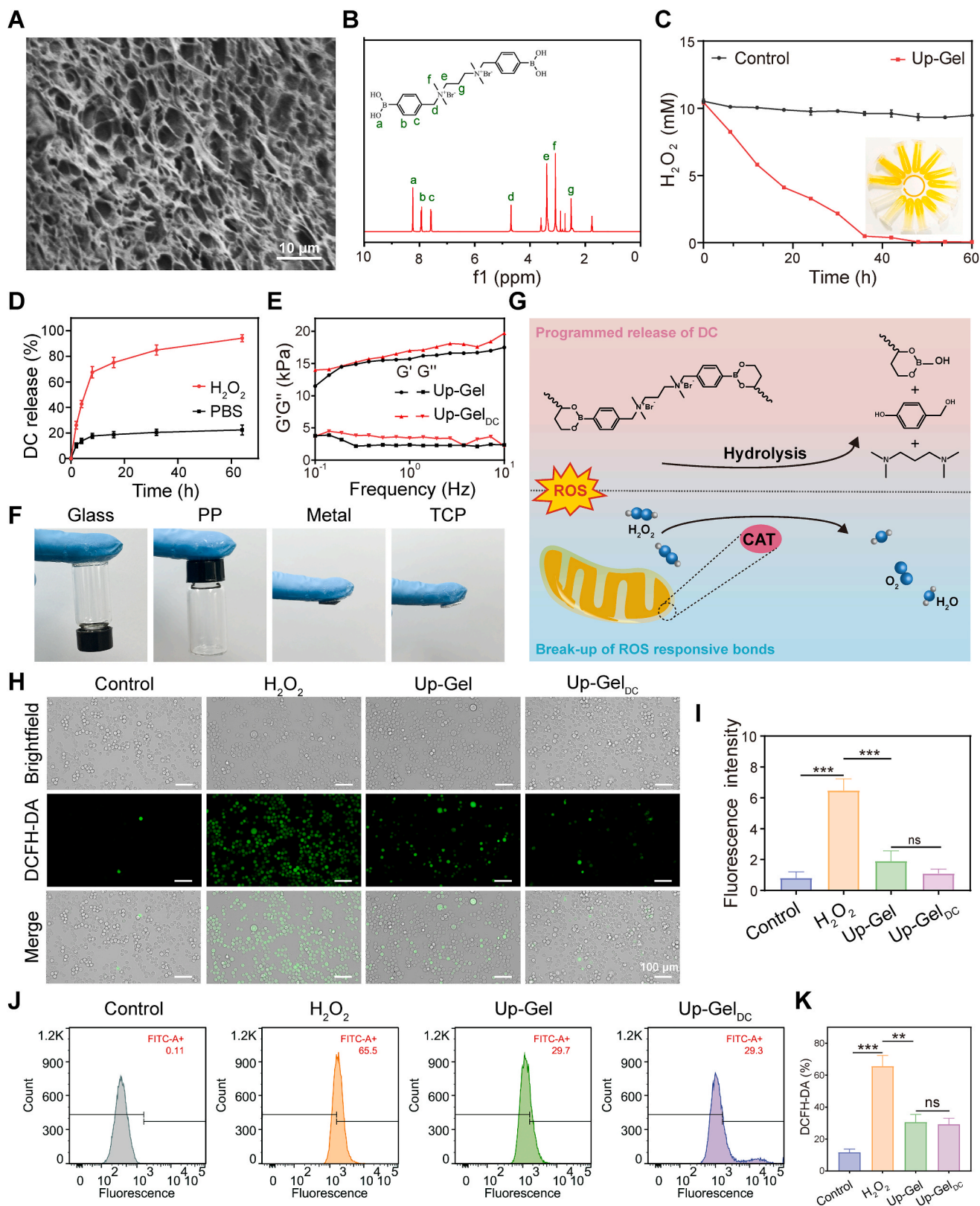


Fig. 2. Characterization of DC-loaded ROS-responsive upper-hydrogel. (A) SEM image of the upper-hydrogel. (B) ^1H NMR of ROS-responsive linker TSPBA. (C) Addition of the upper-hydrogel to H_2O_2 (10 mM) and evaluation of H_2O_2 concentration with titanyl sulfate. (D) Cumulative release of DC from hydrogels in PBS with or without H_2O_2 (10 mM). (E) Storage modulus (G') and loss modulus (G'') of Up-Gel and Up-Gel_{DC} indicate gel-like behavior. (F) Photographs of the upper-hydrogel adhered to various substrates, such as metal and plastic. (G) Mechanism of ROS clearance. (H) Intracellular ROS-scavenging performance of the upper-hydrogel (DCFH-DA⁺; green). (I) Quantification of the fluorescence of DCFH-DA ($n = 3$). (J) Flow cytometry of DCFH-DA labeled RAW264.7 cells on different hydrogel scaffolds in the fluorescein isothiocyanate FITC-A channel. (K) Average fluorescence intensity of DCFH-DA in different groups ($n = 3$). Data are presented as mean \pm SD, ** $p < 0.01$, *** $p < 0.001$.

the lower-hydrogel. Catalase (CAT) was the natural enzyme with the highest content in the human body, playing a powerful role in clearing ROS [35]. The borate ester bond in the upper-hydrogel mainly plays a role similar to CAT enzyme, which can efficiently convert H_2O_2 into H_2O and O_2 (Fig. 2G). DCFH-DA was employed as a probe to determine the intracellular ROS levels of RAW264.7 cells cultured with different hydrogel scaffolds. Apparent fluorescence quenching was more pronounced in the experimental groups than in the positive control group (only with H_2O_2), and the fluorescence intensity was quantified (Fig. 2H and I). The efficiency of the upper-hydrogel in scavenging intracellular ROS was further confirmed using flow cytometry and quantitative analysis (Fig. 2J and K). For the control group and the positive group, the ROS-positive expression rates were 0.11 % and 65.5 %, respectively. In sharp contrast, when Up-Gel, Up-Gel_{DC} were added, the positive expression of ROS was dropped to 29.7 % and 29.3 %, respectively. This

demonstrated that the upper-hydrogel had a good effect in ROS-scavenging, and it was primarily the ROS-responsive junctions that produced a marked effect.

3.2. Exos identification, cellular uptake, and distribution in the lower-hydrogel

Transmission electron microscopy (TEM) revealed that BMSC-derived Exos resembled spherical microvesicles with a size of approximately 100 nm (Fig. 3A). Nanoparticle tracking analysis (NTA) showed that the average size of BMSC-derived Exos was 73.75 ± 12.66 nm, with 99.8 % of Exos falling within the range of 30–150 nm (Fig. 3B). In addition, western blotting results showed that Exos were enriched with surface markers, namely apoptosis-linked gene product 2 interacting protein X (Alix) and tumor susceptibility gene 101 (Tsg101) (Fig. 3C).

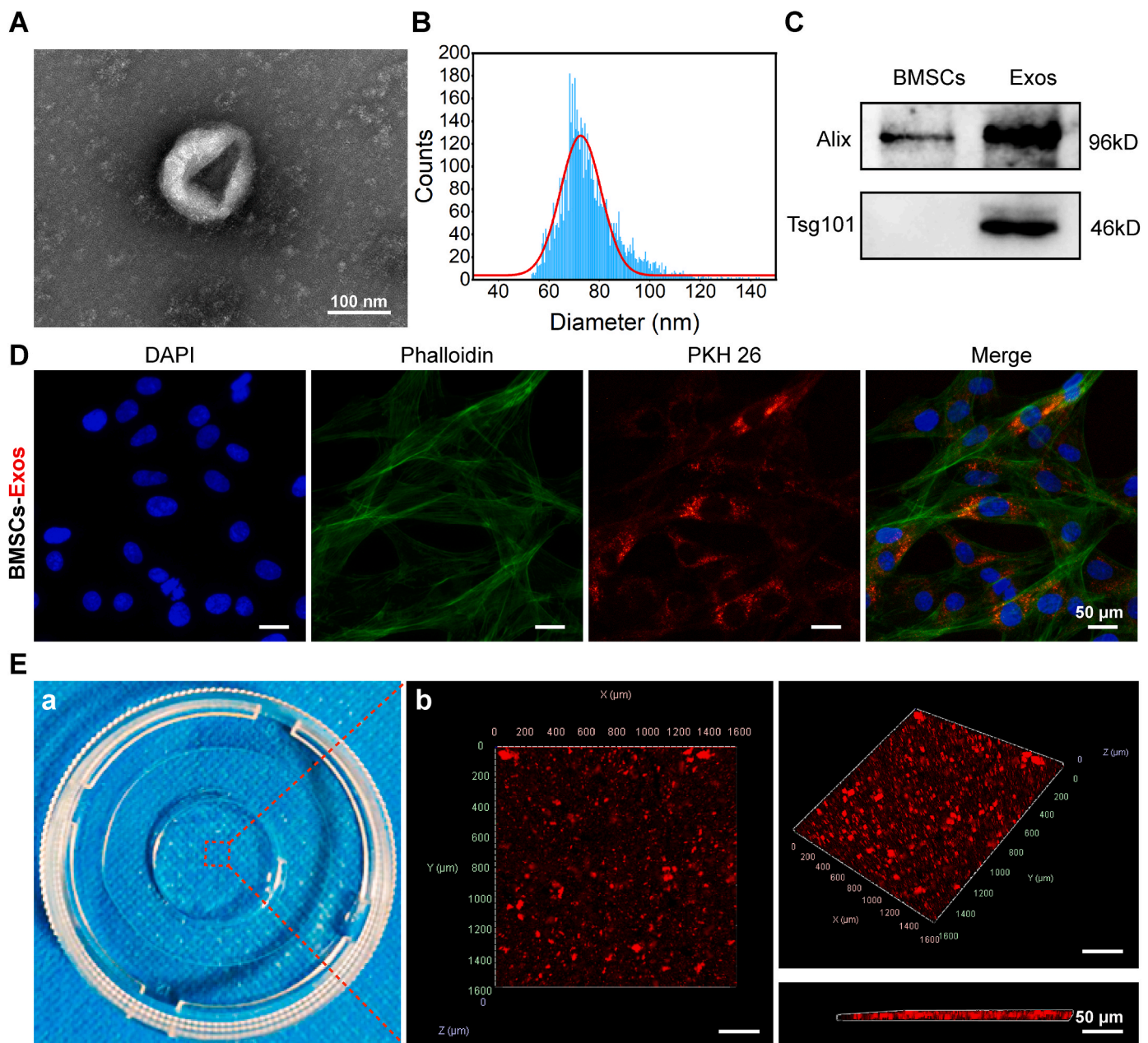


Fig. 3. Isolation, identification, and encapsulation of Exos in Low-Gel_{Exos}. (A) TEM image of BMSC-derived Exos. (B) NTA results of Exos. (C) Western blotting for Alix and Tsg101 in BMSC-derived Exos. (D) Fluorescence image indicating the internalization of Exos by BMSCs. (E) a. Photograph of Low-Gel_{Exos}. b. Exos distribution in Low-Gel_{Exos} showed by confocal microscopy.

These results demonstrated the successful isolation of BMSC-derived Exos. The quantitative western blotting analysis and zeta potential detection of Exos were shown in Fig. S4. Fluorescence imaging showed that BMSCs internalized Exos after the cells were co-cultured with PKH26-labeled Exos for 24 h (Fig. 3D). Physical drawing of Low-Gel_{Exos} and immunofluorescence imaging revealed the 3D spatial distribution of Exos in the hydrogel (Fig. 3E).

3.3. Characterization and cytotoxicity of the lower-hydrogel

In cartilage tissue engineering, different concentrations of HA can have a significant impact on the effectiveness of cartilage repair. According to gene expression testing analysis, the effectiveness of cartilage formation is higher in the concentration range of 0.5–5 % [36]. Among them, the concentration of about 2 % is very similar to the natural HA content in the joint environment [37]. Considering the clinical situation and safety, we used 0.5 %, 1 % and 2 % HA concentrations (HA/SA = 1:4, 1:2, 1:1) to screen the lower-hydrogel scaffold loaded with Exos. SEM images showed that all hydrogels had uniform interconnected porous structures, the pore size increased gradually as the proportion of HA in the hydrogel mixture increased (Fig. 4A and B). The EDS mapping results showed an even cross-linked network of the hydrogel by the gelation sodium alginate with calcium ions, favoring the uniform distribution of Exos encapsulated (Figs. S5A and B). The all-prepared hydrogels exhibited a stable viscoelastic property with greater storage modulus (G') and smaller loss modulus (G''), as shown in the frequency-scan curves in the rheological test (Fig. 4C). The elasticity of the hydrogels was considered to be increased as the HA content increased, demonstrating the higher cross-link density of with larger amount of HA. This mechanical stability could provide structural support for the damaged cartilage, transmit mechanical forces effectively, and maintain the shape and integrity during the healing process of joint cartilage [38]. Hydrogel swelling compresses the surrounding tissues and might even lead to separation from the target organ. Experimental data showed that the SR decreased as the proportion of HA in the hydrogel mixture increased, which was related to the ionic strength balance between polyanions and polycations in the hydrogel mixture (Fig. 4D) [39]. Subsequently, we characterized the release of Exos encapsulated in the prepared hydrogels, revealing about 80 % of Exos were released within 14 days. The rate of Exos release slightly increased as the proportion of HA in the hydrogel mixture increased (Fig. 4E). Because the lower-hydrogel was designed to support cell infiltration, the biocompatibility of the prepared hydrogels was evaluated. Live/dead staining indicated that the hydrogels were biocompatible with BMSCs. Furthermore, increasing the HA content substantially improved the biocompatibility of the hydrogel (Fig. 4F and G). Additionally, the effect of the hydrogels on the proliferation of BMSCs was determined using CCK-8. As shown in Fig. 4H, there was a significant difference in cell viability between the hydrogel groups and the control group after 1, 2, and 3 days of culturing. Examination of the three hydrogel groups showed the hydrogel with the higher HA content promoted more pronounced cell proliferation.

During cartilage regeneration, new granulation tissue needs space to grow, gradually replacing the implanted scaffold [40]. In this study, the HA/SA (1:1) group had the largest pore size structure and did not produce significant differences in other physicochemical properties. According to a previous study, increasing the HA content of HA-based hydrogels enhances chondrogenesis and ECM deposition of coated mesenchymal stem cells [41]. Indeed, the biocompatibility of the prepared hydrogels with BMSCs was positively correlated with the proportion of HA. Considering the above results, we used the HA/SA ratio of 1:1 to prepare the lower-hydrogel as the carrier of Exos.

In order to obtain structurally stable scaffolds of bilayer-hydrogel, we adopted repeated freeze-thawing for the binding of the upper and lower hydrogel layers. The optical images before and after stretching the bilayer-hydrogel showed that the final fracture occurred in the upper

layer rather than at the interface, demonstrating the strong bonding strength between the two layers (Fig. 4I). The interface microstructure observed by SEM showed that the two layers was connected continuously with no obvious boundary between the two layers and the macro and micro pores structure of the two layers transitioned smoothly (Fig. 4J). The degradation and release behavior curves of the bilayer-hydrogel were shown in Fig. 4K, L, where about 90 % of the upper-hydrogel were degraded and DC drug showed an initial burst release within the first 3 days. Subsequently, the lower-hydrogel degradation as well as the release of Exos was accelerated gradually, with approximately 90 % of Exos released by around 25 days. DC release from the upper-hydrogel was rapid and prioritized, capable of swiftly improving the inflammatory environment and providing a favorable microenvironment for the release of Exos.

3.4. Effects of upper-hydrogel on inflammation through immunomodulation

Macrophages are primary mediators of inflammation after injury, and the production of ROS has a significant effect on the polarization of macrophages, as depicted in Fig. 5A. The effect of the upper-hydrogel on RAW264.7 polarization *in vitro* was investigated. In particular, the expression of relevant inflammatory molecules was analyzed using qPCR, immunofluorescence, and flow cytometry. qPCR results indicated that the Up-Gel_{DC} group efficiently down-regulated the expression of M1 phenotypic markers (*IL-1 β* , *IL-6*, *iNOS*) and up-regulated the expression of M2 phenotypic markers (*IL-10*, *Arg-1*, *CD206*) compared with the control group (Fig. 5B). In alignment qPCR findings, immunofluorescence results indicated that the percentage of iNOS-positive cells was lower in the Up-Gel_{DC} group than in the control group, while the percentage of Arg-1-positive cells was higher in the Up-Gel_{DC} group than in the control group (Fig. 5C and D). Flow cytometry using CD86 as a marker of M1 phenotype showed that the fluorescence of 59.9 % of LPS-treated cells was stronger than the background fluorescence, and 38.8 % and 23.2 % of cells were retained in the M1 region after Up-Gel and Up-Gel_{DC} treatments, respectively (Fig. 5E). To determine the effect of the upper-hydrogel on the M2 phenotype, we examined CD206 expression using flow cytometry. The results showed that the Up-Gel_{DC} group had the highest number of CD206-positive cells (more than IL-4-treated cells) among the tested groups, including the IL-4-treated group (Fig. 5F). Our findings demonstrated the potent immunomodulatory effects of the upper-hydrogel. In particular, the upper-hydrogel effectively inhibited macrophage M1 polarization and promoted M2 polarization.

3.5. Effect of bilayer-hydrogel on chondrogenic differentiation and chondroprotection *in vitro*

In order to investigate the effect of the bilayer-hydrogel on the chondrogenic differentiation of BMSCs. We first verified the ability of the lower-hydrogel to recruit (Fig. S6) and adhere (Fig. S7) to BMSCs. The addition of Exos significantly increases BMSCs migration and adhesion ability. Subsequently, BMSCs were treated with the bilayer-hydrogel for 7 and 14 days, followed by qPCR assessments. qPCR results showed that the expressions of *Col II*, *Sox9*, and *ACAN* mRNA were significantly enhanced upon the addition of upper-hydrogel to Bil-Gel_{DC/Exos} (Fig. 6A). Western blotting results were consistent with qPCR results (Fig. 6B and C). The main constituents of cartilage ECM, proteoglycans and type II collagen (COL II), were analyzed using Alcian blue staining and immunofluorescence, respectively. Alcian blue staining showed that proteoglycan expression (blue color) increased sequentially in the order of Control, Up-Gel_{DC}, Low-Gel_{Exos}, and Bil-Gel_{DC/Exos} groups (Fig. 6D). Immunofluorescence staining for COL II and ACAN in the four groups resulted in images with intense green and red fluorescence, indicating that Bil-Gel_{DC/Exos} enhanced cartilage differentiation (Fig. 6E and F). This experiment showed that the expression of

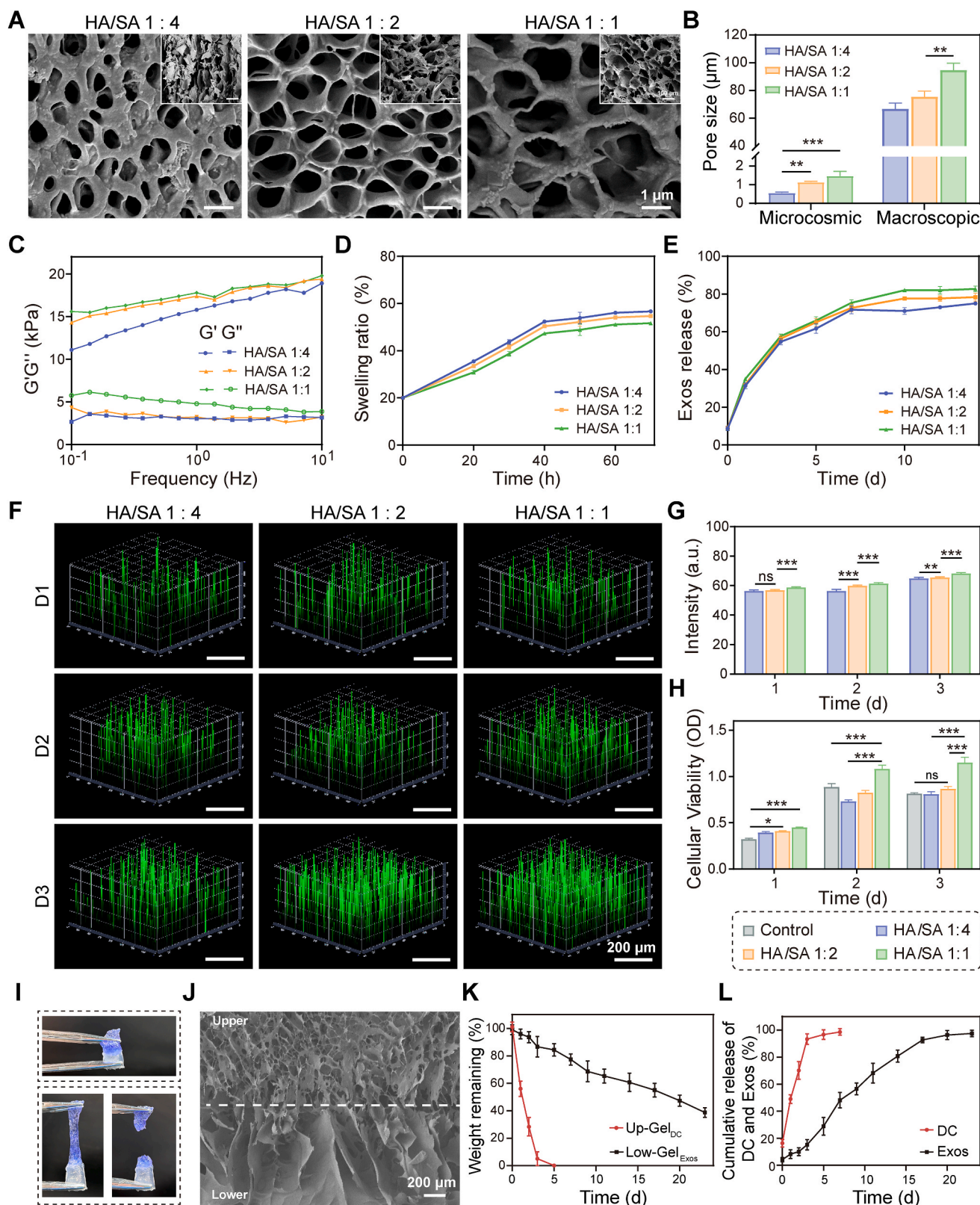


Fig. 4. Characterization of lower-hydrogel with different HA contents and proliferation of encapsulated BMSCs. (A) SEM images of fabricated hydrogels showing micropores in the hydrogel matrix. (B) Average pore size of fabricated hydrogels based on SEM images ($n = 3$). (C) Storage modulus (G') and loss modulus (G'') of hydrogels indicate gel-like behavior ($n = 3$). (D) Swelling ratio of hydrogels with different HA contents ($n = 3$). (E) Release of Exos from hydrogels with different HA contents ($n = 3$). (F) Activity of BMSCs in hydrogels observed by 2.5D imaging. (G) Quantification of fluorescence from the live/dead assay. (H) CCK-8 assay of each group after 1, 2, and 3 days of cell culturing ($n = 5$). (I) Optical images of the bilayer-hydrogel before and after the stretching, presenting the strong binding force at the interface. (J) SEM images of the bilayer-hydrogel. (K) The degradation behaviors of Up-Gel_{DC} and Low-Gel_{EXOS}. (L) The release behaviors of bilayer-hydrogel. Data are presented as mean \pm SD, * $p < 0.05$, ** $p < 0.01$, *** $p < 0.001$.

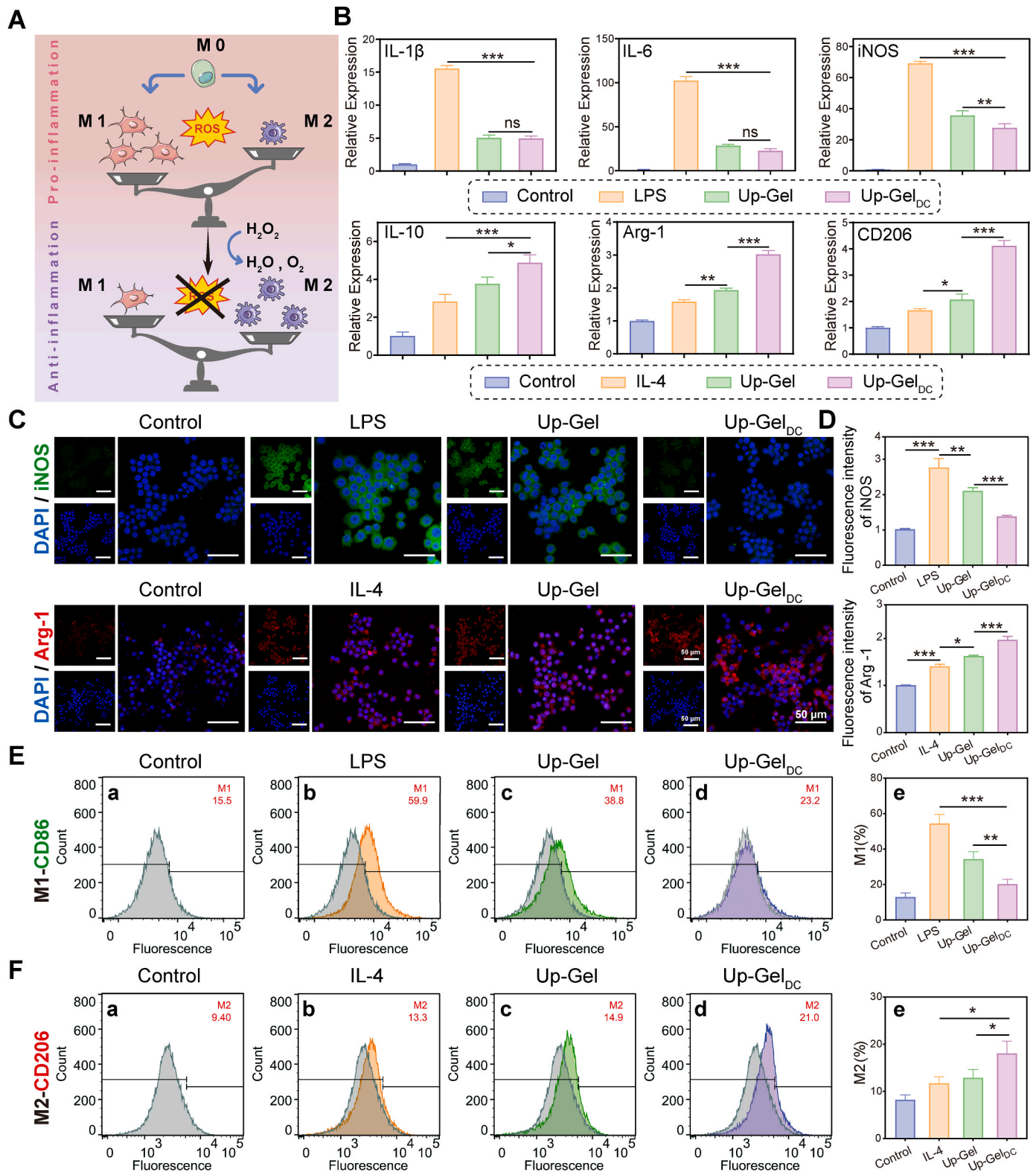


Fig. 5. Effect of upper-hydrogel treatment on macrophage polarization and inflammation-related gene expression *in vitro*. (A) Schematic diagram of the effect of ROS clearance on RAW264.7 polarization. (B) qPCR evaluation of the expression of pro-inflammatory factors (*IL-1 β* , *IL-6*, *iNOS*) and anti-inflammatory factors (*IL-10*, *Arg-1*, *CD206*) in RAW264.7 cells treated with different hydrogel scaffolds ($n = 3$). (C) Fluorescence images showing iNOS (green) and Arg-1 (red) in RAW264.7 cells 48 h after inflammation stimulation. (D) Quantitative analysis of the fluorescence of iNOS and Arg-1 in each group ($n = 3$). (E) (a–d) Flow cytometry histograms for CD86. (e) Average fluorescence intensity of CD86 in different groups ($n = 3$). (F) (a–d) Flow cytometry histograms for CD206. (e) Average fluorescence intensity of CD206 in different groups ($n = 3$). Data are presented as mean \pm SD, * $p < 0.05$, ** $p < 0.01$, *** $p < 0.001$.

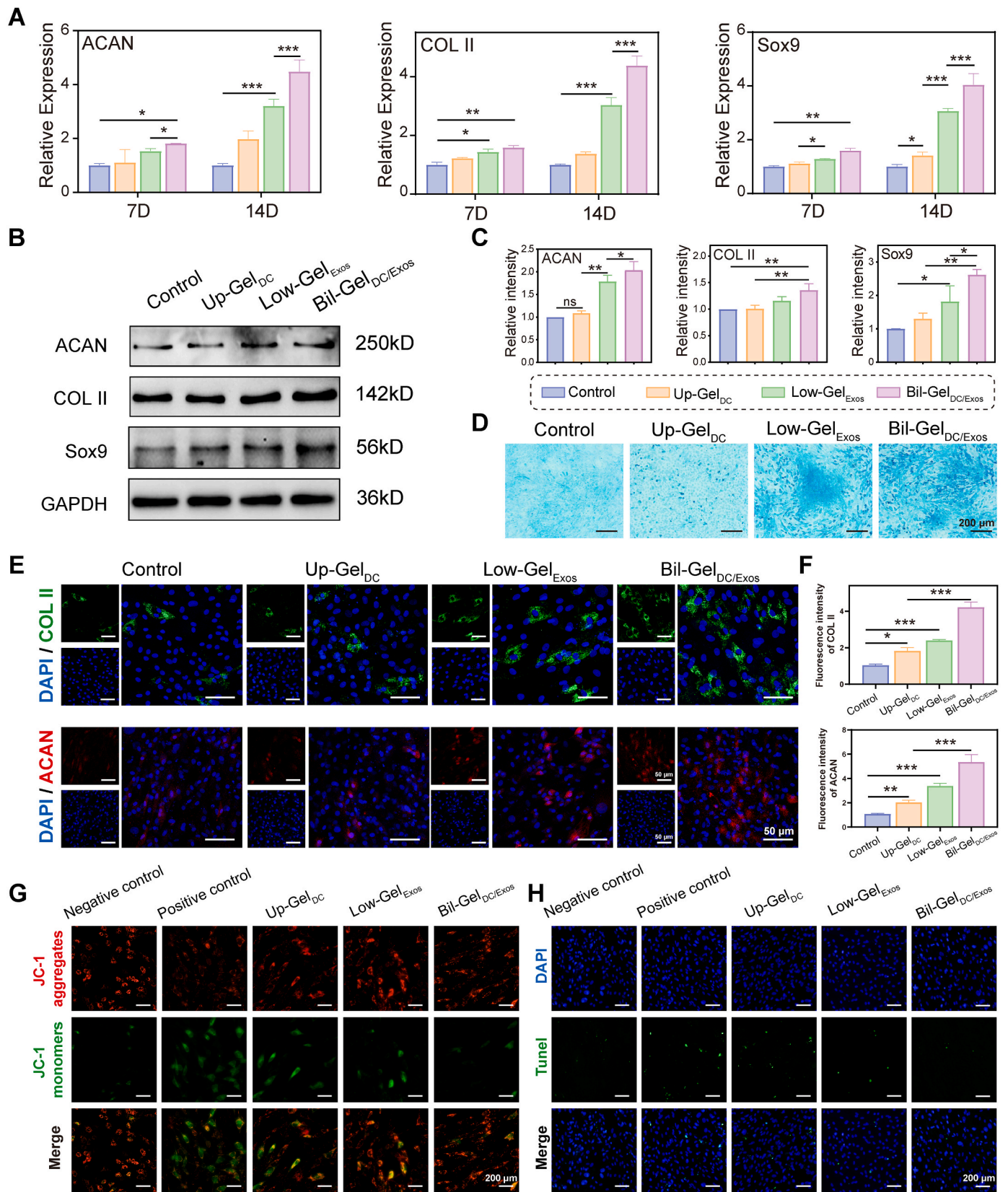


Fig. 6. Effect of Bil-Gel_{DC/Exos} adhesive hydrogel on BMSCs differentiation and chondroprotection. (A) qPCR evaluation of the mRNA expression of COL II, Sox9, and ACAN in BMSCs treated with Bil-Gel_{DC/Exos} extract for 7 and 14 days ($n = 3$). (B) Western blotting for ACAN, COL II, and Sox9 in BMSCs treated with Bil-Gel_{DC/Exos} extract for 7 days. (C) Quantitative analysis of western blotting results ($n = 3$). (D) Alcian blue staining of proteoglycans in BMSCs treated with Bil-Gel_{DC/Exos} extract for 7 days. (E) Immunofluorescence staining for COL II and ACAN in BMSCs treated with Bil-Gel_{DC/Exos} extract for 7 days. (F) Quantitative analysis of the fluorescence of COL II and ACAN in each group ($n = 3$). (G) JC-1-based immunofluorescence assay of chondrocytes. (H) Detection of apoptotic articular chondrocytes using the TUNEL assay. Data are presented as mean \pm SD, * $p < 0.05$, ** $p < 0.01$, *** $p < 0.001$.

chondrocyte marker protein in BMSCs continuously improved with the upper-hydrogel in the bilayer-hydrogel and the addition of Exos. This result suggested that the Bil-Gel_{DC/Exos} was able to improve chondrocyte formation and differentiation, and also indicated the necessity of the presence of an upper-hydrogel.

The inflammatory environment following AC injury affects not only the chondrogenic differentiation of BMSCs but also the degeneration of surrounding chondrocytes. IL-1 β is a major catabolic cytokine of cartilage injury and is involved in the stimulation of catabolic enzymes, such as MMP, which degrades the ECM of cartilage and leads to the release of GAG [42]. We used IL-1 β to simulate cartilage injury *in vitro* and then investigated the effect of Bil-Gel_{DC/Exos} on chondrocyte apoptosis. Early cell apoptosis was assessed by measuring the mitochondrial membrane potential with JC-1. The findings indicated that the Bil-Gel_{DC/Exos} group

counteracted IL-1 β -induced mitochondrial damage (Fig. 6G). In addition, the TUNEL assay revealed a significant reduction in apoptotic cells in the Bil-Gel_{DC/Exos} group compared with the control group, indicating that Bil-Gel_{DC/Exos} provided chondroprotection (Fig. 6H). The corresponding quantification was shown in Fig. S8.

3.6. *In vivo* evaluation of ROS-scavenging and inflammatory regulation

To verify the ROS scavenging capability of bilayer-hydrogel *in vivo*, the ROS-specific chemiluminescence probe was injected to detect the expression level of ROS. As shown in Fig. 7A and B, the ROS level was consistently higher in the control group than in the Bil-Gel_{DC/Exos} group, and the chemiluminescence signal was significantly attenuated after bilayer-hydrogel treatment, indicating that ROS expression was

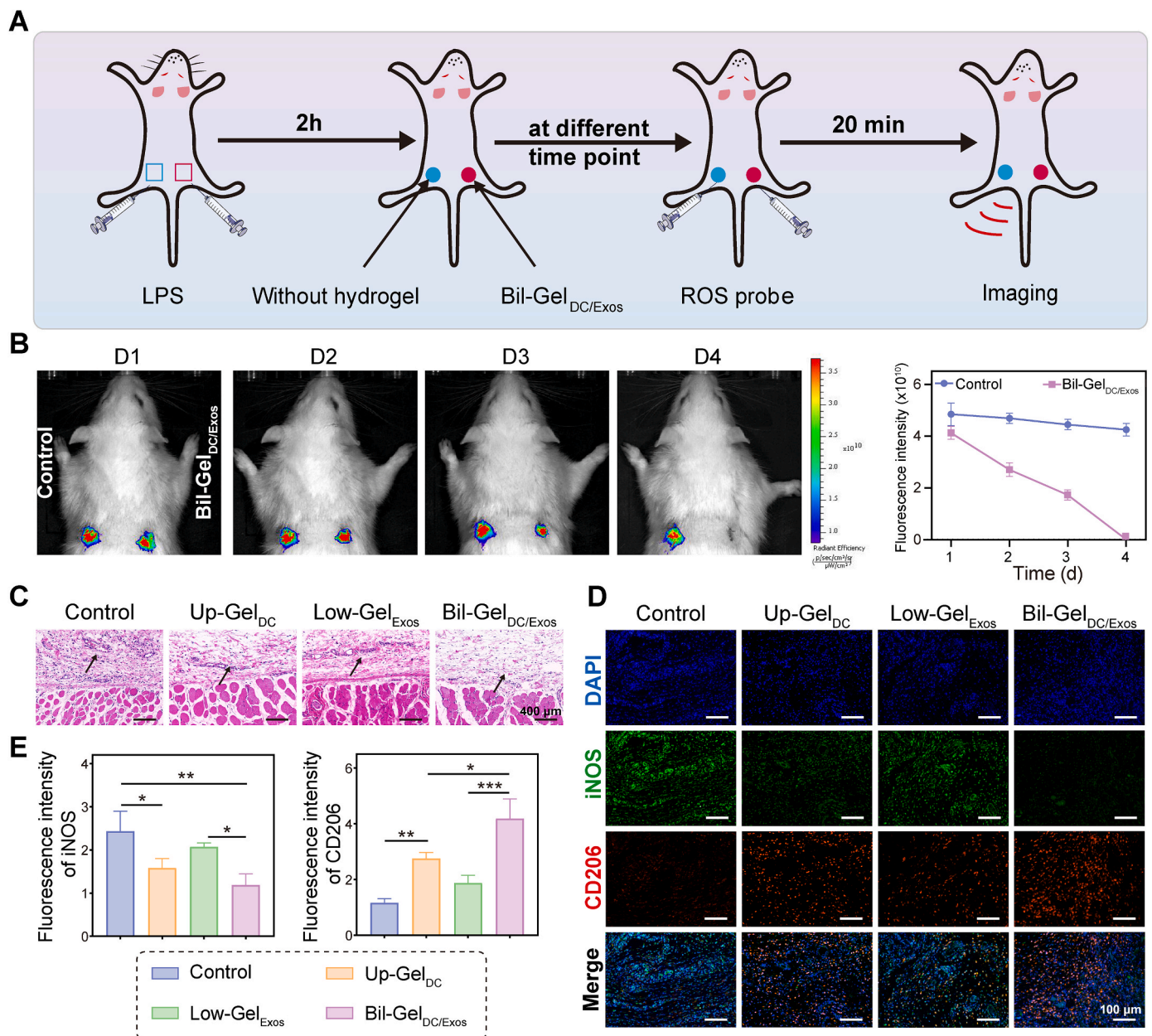


Fig. 7. ROS clearance and inflammation inhibition induced by implantation of various materials *in vivo*. (A, B) Interactive video information system (IVIS) images of *in vivo* ROS clearance and relative fluorescence intensity ($n = 3$). (C) H&E staining of dorsal skin implanted with different hydrogels. (D) Immunofluorescence staining for pro-inflammatory M1 biomarker (iNOS; green) and anti-inflammatory M2 biomarker (CD206; red) in the dorsal skin after the implantation of different hydrogels. (E) Quantitative analysis of the fluorescence of iNOS and CD206 in each group ($n = 3$). Data are presented as mean \pm SD, * $p < 0.05$, ** $p < 0.01$, *** $p < 0.001$.

significantly inhibited. Subsequently, the major organs (heart, liver, spleen, lungs, and kidneys) were collected and their H&E staining results demonstrated that Bil-Gel_{DC/Exos} did not induce significant abnormalities or organ damage compared with the control group (Fig. S9).

The anti-inflammatory and pro-inflammatory pathways in the local microenvironment are closely related to activated macrophages, which can produce excessive ROS and inflammatory factors within cells [43]. Therefore, the phenotypic transition of macrophages was assessed via the H&E and immunofluorescence staining. H&E staining showed that the tissue surrounding Bil-Gel_{DC/Exos} contained reduced inflammatory cells and well-organized collagen fibers (Fig. 7C). The Low-Gel_{Exos} group exhibited anti-inflammatory effects, but its effectiveness in rapidly improving the inflammatory environment was not as pronounced as the Up-Gel_{DC} group. Moreover, the Bil-Gel_{DC/Exos} group demonstrated the most effective anti-inflammatory outcomes. This suggested that although Exos possessed inflammatory regulatory capabilities, their functional impact in swiftly ameliorating the inflammatory environment was limited, highlighting the need for adjunctive anti-inflammatory drugs. Consistent with the results of H&E staining, immunofluorescence staining revealed that Bil-Gel_{DC/Exos} significantly suppressed the expression of M1 macrophage marker iNOS and promoted the expression of anti-inflammatory M2 macrophage marker CD206 (Fig. 7D and E). The results demonstrated that the addition of the upper-hydrogel can inhibit inflammation more effectively and trigger the alteration of macrophage phenotypes *in vivo*.

3.7. Cartilage repair after regulating the inflammatory environment *in vivo*

Cartilage defects were created in the patellofemoral groove of rats to assess cartilage regeneration *in vivo* (Fig. S10). Cartilage repair was evaluated at different time points using MRI (Fig. 8A). The four groups were evaluated by assessing tissue regeneration within the defect, tissue integration with the surrounding cartilage, subchondral bone signals, intra-articular inflammation, and peripheral cartilage degeneration. In the control group, defects were filled with disorganized regenerative tissue, and an abnormally intense shadow was observed in the subchondral bone at both 4 and 8 weeks. In the Up-Gel_{DC} group, the defect area was extensively filled, although tissue integration with the surrounding cartilage was suboptimal. In the Low-Gel_{Exos} group, the cartilage defect area was filled with regenerated tissue, which was poorly fused with the surrounding cartilage. In the Bil-Gel_{DC/Exos} group, the regenerated defect area was effectively fused with the surrounding tissue, demonstrating superior repair outcomes at both 4 and 8 weeks compared with the other three groups. The distal femurs were collected for gross observation (Fig. 8B) and graded in accordance with ICRS (Fig. S11A). The average ICRS grading score of the Bil-Gel_{DC/Exos} group was significantly higher than those of the control, Up-Gel_{DC}, and Low-Gel_{Exos} groups at 4 and 8 weeks. These findings indicated that Bil-Gel_{DC/Exos} efficiently repaired cartilage defects without dislodging during joint motion.

H&E (Fig. S12) and SOFG (Fig. 8C) were used to identify histological changes in the cartilage and determine histological scores (Fig. S11B). In the control group, the patellofemoral groove defect was filled with neofibrous tissue without the formation of new cartilage (red stained). In the Bil-Gel_{DC/Exos} group, new cartilage formed in the defect at 4 weeks postoperation, and the cartilage surface at 8 weeks postoperation was similar to normal tissue. In the Bil-Gel_{DC/Exos} group, TB staining showed that the thickness of repaired tissue gradually increased over time, and the ECM of regenerated cartilage was uniform (Fig. 8D). The expressions of ECM proteins in defective and new cartilage were analyzed using immunofluorescence and immunohistochemistry. The expressions of ACAN and COL II were higher in the Bil-Gel_{DC/Exos} group than in the other groups (Fig. 8E and F) and corresponding quantification shown in Fig. S13. To further clarify the specific type of collagen, immunohistochemical staining was performed on COL I (Fig. S14). The results were

consistent with H&E, SOFG and TB. Bil-Gel_{DC/Exos} treatment was able to produce less type I collagen. It showed that the cartilage was able to regenerate well without fibrosis. In summary, Bil-Gel_{DC/Exos} facilitated cartilage repair from as early as 4 weeks postoperation, which was not achieved with either Up-Gel_{DC} or Low-Gel_{Exos}.

3.8. Mechanism of Bil-Gel_{DC/Exos} enhanced cartilage regeneration

Owing to deficiencies in chondrocyte replication and proliferation, cartilage regeneration is dependent on the migration of endogenous BMSCs to defect sites and differentiation of BMSCs into chondrocytes [44]. We performed RNA sequencing (RNA-seq) to analyze gene expression during cartilage regeneration in the presence of Bil-Gel_{DC} and Bil-Gel_{DC/Exos}. Differential expression gene analysis showed that 1174 genes were up-regulated and 1061 genes were down-regulated in BMSCs in the Bil-Gel_{DC/Exos} groups compared with the Bil-Gel_{DC} group ($p < 0.05$, $|\log_2FC| > 1$) (Fig. S15A). The up-regulated and down-regulated genes of the two groups are shown in the volcano plot, along with statistical analysis (Fig. 8G). Furthermore, KEGG enrichment analysis revealed that several pathways related to ECM metabolism were activated, while the Wnt pathway was inhibited in the Bil-Gel_{DC/Exos} group (Fig. 8H). In particular, Bil-Gel_{DC/Exos} regulated the expression of key genes associated with the chondrogenic differentiation of BMSCs cells, such as *TGF β 3*, *Smad7*, *CLK2*, *TCF4*, *TCF7*, and *DYRK1A*, of which *CLK2* inhibits the induction of early cartilage formation and *DYRK1A* inhibits the enhancement of mature chondrocyte function [45]. In addition, the expressions of *TCF4* and *TCF7*, chondrogenic genes in the Wnt pathway, were also inhibited (Fig. 8I). qPCR was used to verify the results of KEGG analysis (Fig. S15B). The levels of four down-regulated genes were lower in the Bil-Gel_{DC/Exos} group than in the Bil-Gel_{DC} group, which was consistent with the RNA-seq results.

In summary, these results indicated that Bil-Gel_{DC/Exos} modulated chemokine signaling pathways to promote the differentiation of BMSCs into chondrocytes. In contrast to conventional hydrogels loaded with bioactive molecules, natural Exos were used in this study to promote the migration, retention, and differentiation of BMSCs. However, the exact mechanism of chemokine pathway activation remains to be explored in future studies.

4. Discussion

The cartilage repair process consists of the hemostasis stage, inflammation stage, proliferation stage, and maturation stage. During the inflammation stage, a strong inflammatory response delays the repair process, while appropriate inflammatory reactions initiate the proliferation stage and create a favorable microenvironment, which accelerates the entire wound healing process [46]. In this study, we designed a ROS-responsive Exos-loaded bilayer-hydrogel to provide multi-staged treatment, thereby optimizing the therapeutic effect of Exos for cartilage regeneration.

The bilayer-hydrogel releases sodium diclofenac (DC) early for immunomodulation and exosomes (Exos) later to match the activation cycle of cartilage repair. In a simulated environment with elevated levels of ROS, the upper-hydrogel degraded completely in a short period of time. This rapid degradation plays a vital role in rapidly modulating the inflammatory environment, thereby reducing additional damage to the ECM. The regeneration of cartilage defects begins with the capture of macrophages in the fibrous network of the defect area, which modulates the inflammatory response for the recruitment of endogenous BMSCs from the marrow cavity of the subchondral bone [47]. Subsequently, these recruited BMSCs proliferate and differentiate into chondrocytes at the wound site. Then, synthesized COL II and proteoglycans rebuild the cartilage ECM, thereby contributing to the regeneration of cartilage tissue [48]. Inflammation proves to be a double-edged sword for tissue regeneration [49]. Typically, during the initial recovery phase, the inflammatory response defends against interference from external

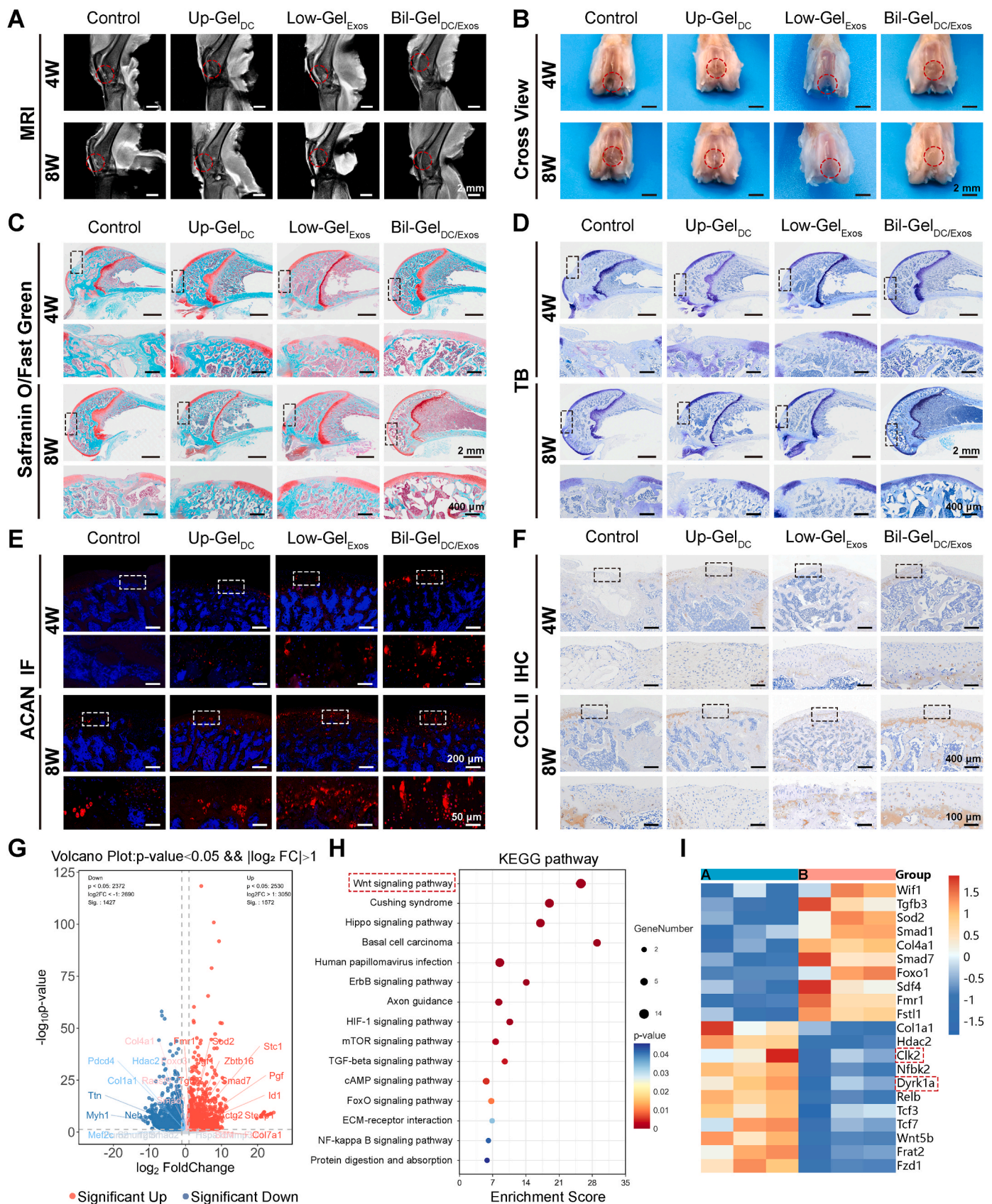


Fig. 8. Evaluation of cartilage defect repair and regeneration mechanisms. (A) MRI-based evaluation of cartilage defects. (B) Macroscopic observation of cartilage defects at different time points. (C) SOFG staining of rat knees at 4 and 8 weeks after hydrogel implantation. (D) Toluidine blue staining of repaired cartilage at 4 and 8 weeks postoperation. (E) Immunofluorescence staining for ACAN in cartilage at 4 and 8 weeks postoperation. (F) Immunohistochemistry for COL II in the knee cartilage defect at 4 and 8 weeks postoperation. (G) RNA sequence analysis of BMSCs treated with Bil-Gel_{DC} and Bil-Gel_{DC/Exos} extracts. (H) KEGG analysis of RNA sequences. (I) Heat map of migrating genes (A: Bil-Gel_{DC}; B: Bil-Gel_{DC/Exos}).

microorganisms and promotes the degeneration of phagocytes in the damaged tissue. However, uncontrolled inflammation limits the recovery of damaged tissue [50]. Excessive ROS within the wound not only triggers a strong inflammatory response but also impairs endogenous stem cells and macrophages [51]. ROS, as an important inflammatory factor, can activate macrophages, thereby seriously exacerbating the inflammatory response [52]. Thus, the targeted reduction of overexpressed ROS and the regulation of activated macrophage phenotypes could substantially mitigate the inflammatory response. An excessive host inflammatory response leads to cartilage fibrosis, and thus it is critical to create an appropriate host inflammatory environment for hyaline cartilage tissue formation [53]. Under the synergistic antioxidant and anti-inflammatory effects of the upper-hydrogel, inflammatory cytokines produced by pro-inflammatory immune cells, such as *IL-1 β* , *IL-6*, and *iNOS*, were significantly down-regulated, and inflammatory cytokines produced by anti-inflammatory immune cells, such as *IL-10*, *Arg-1*, and *CD206*, were rapidly up-regulated. This indicated that Up-Gel_{DC} can create the anti-inflammatory environment required for tissue repair and regeneration.

The continuous release of Exos from the hydrogel plays a pivotal role in facilitating the migration of BMSCs, thus compensating for deficiencies in chondrocyte replication and proliferation [44]. For the construction of the lower-hydrogel, we chose to combine SA with HA. In addition to its biocompatibility, SA exhibited properties such as fast cross-linking with divalent metal interactions [54]. And it could combine with PVA through physical interactions such as hydrogen bonding and polymer chain entanglement to enhance the stability of the connection with the upper-hydrogel. When we optimized the HA content (HA/SA ratio of 1:1) of the lower-hydrogel, we found that increasing the HA/SA ratio also increased the cytocompatibility and pore size of the formed hydrogel with higher Exos release. The large pores of the scaffold provide infiltration channels for stem cell migration, cellular nutrient transportation, and waste elimination [55]. Nevertheless, the harsh microenvironment at the injury site is characterized by high levels of ROS and excessive inflammation, which disrupts the biological activity required for recruiting BMSCs. Although Exos are credited with some of immunomodulation, their therapeutic effect on cartilage repair separately was less productive than we anticipated under pro-inflammatory environment, as presented in results of subcutaneous implantation (Fig. 7C and D). Hence prior to Exos release, the upper-hydrogel loaded with DC was driven to act as a protective umbrella for the lower-hydrogel encapsulated Exos through rapidly and effectively capturing excess ROS and reprogramming macrophages phenotype. The *in vitro* findings indicated that the upper-hydrogel promoted chondrogenic differentiation in an inflammatory environment and that this effect was further enhanced by the addition of Exos. Moreover, the bilayer-hydrogel inhibited chondrocyte apoptosis, thereby protecting the limited amounts of chondrocytes. *In vivo* experiments showed that the control group only produced disordered fibrous tissue, with almost no spontaneous transformation into transparent cartilage. In contrast, the Bil-Gel_{DC/Exos} group completely replaced the defect with newly formed, uniform cartilage tissue at only 8 weeks postoperation. In addition, with the gradual degradation of the upper-hydrogel and the release of Exos, the cartilage repair effect became more pronounced. This indicated that upper-hydrogel regulates inflammation and makes the cartilage repair effect more pronounced. On the basis of these findings, we explored the relevant mechanisms of enhanced cartilage repair and Exos function. Bioinformatics analysis indicated that the expressions of genes involved in ECM degradation were suppressed, while the expressions of genes related to cartilage repair were promoted in the Bil-Gel_{DC/Exos} group compared with the Bil-Gel_{DC} group. Enrichment analysis of the KEGG pathway indicated inhibition of the Wnt signaling pathway, which plays an important role in cartilage repair [56]. However, the exact mechanism of Exos enhanced cartilage repair in an improved inflammatory environment still requires further exploration.

In summary, ROS overproduction and M1/M2 imbalance form a vicious cycle and lead to an inflammatory microenvironment. Whereas the persistence of an inflammatory environment is a major obstacle to cartilage repair, this may limit the success of strategies to recruit endogenous cells and use Exos scaffolds for *in situ* cartilage repair [57]. In the present study, we prepared a ROS-responsive Exos-loaded bilayer-hydrogel scaffold. DC released upon the degradation of the upper-hydrogel reduced endogenous ROS production, promoted M2-type polarization of macrophages, and regulated the inflammatory microenvironment in multiple dimensions. This design broke the vicious cycle of the inflammatory milieu and provided a greenhouse for the recruitment and activation of proliferative BMSCs as well as chondroprotection for enhanced cartilage repair. Taken together, the bilayer-hydrogel displays promise for further clinical validation.

5. Conclusions

A ROS-responsive Exos-loaded bilayer-hydrogel was developed to promote cartilage repair. The results of *in vitro* and *in vivo* experiments show that the Bil-Gel_{DC/Exos} hydrogel has an obvious role in inhibiting inflammation and promoting cartilage formation in the damaged cartilage environment. The bilayer-hydrogel overcomes the shortcomings of traditional single-stage therapies by closely linking two different repair stages in a phased treatment, as well as harvests Exos as therapeutic drug optimally. We believe this study provides a promising hydrogel design for the treatment of cartilage defects.

Ethics approval and consent to participate

All procedures adhered to the National Institutes of Health (NIH) Guide for the Care and Use of Laboratory Animals, and received approval from the Animal Ethics Committee of Shandong Provincial Hospital Affiliated to Shandong First Medical University (No. 2023-013).

Declaration of competing interest

All the authors declare no conflict of interest.

CRediT authorship contribution statement

Xiaoqing Lu: Writing – review & editing, Writing – original draft, Visualization, Validation, Methodology, Investigation, Formal analysis, Data curation, Conceptualization. **Shimin Dai:** Writing – review & editing, Methodology, Conceptualization. **Benzhao Huang:** Validation, Investigation, Formal analysis. **Shishuo Li:** Methodology, Data curation. **Peng Wang:** Methodology, Data curation. **Zhibo Zhao:** Methodology, Formal analysis. **Xiao Li:** Investigation, Formal analysis. **Ningbo Li:** Visualization. **Jie Wen:** Visualization. **Yunhan Sun:** Visualization. **Zhentao Man:** Visualization, Conceptualization. **Bing Liu:** Visualization, Validation, Supervision, Methodology, Investigation, Formal analysis, Conceptualization. **Wei Li:** Supervision, Formal analysis, Conceptualization.

Acknowledgments

This work was supported by National Natural Science Foundation of China (Nos. 52002223, 81672185 and 81702152), Key Technology Research and Development Program of Shandong (Major Science and Technology Innovation Project) (2020CXGC010502), Taishan Scholar Foundation of Shandong Province (No. tsqn202211348), and the Shandong Province Natural Science Foundation (Grant Nos. ZR2022MH222 and ZR2023MH209).

Appendix A. Supplementary data

Supplementary data to this article can be found online at <https://doi.org/10.1016/j.bioactmat.2024.04.017>.

References

- [1] D. Chen, J. Shen, W. Zhao, T. Wang, L. Han, J.L. Hamilton, H.-J. Im, Osteoarthritis: toward a comprehensive understanding of pathological mechanism, *Bone Res* 51 (2017), <https://doi.org/10.1038/boneres.2016.44>.
- [2] X. Shang, X. Hao, W. Hou, J. Liu, R. Chi, X. Deng, C. Pan, T. Xu, Exercise-induced modulation of myokine irisin on muscle-bone unit in the rat model of post-traumatic osteoarthritis, *J. Orthop. Surg. Res.* 191 (2024) 49, <https://doi.org/10.1186/s13018-024-04532-2>.
- [3] S. Liu, C. Zhang, Y. Zhou, F. Zhang, X. Duan, Y. Liu, X. Zhao, J. Liu, X. Shuai, J. Wang, Z. Cao, MRI-visible mesoporous polydopamine nanoparticles with enhanced antioxidant capacity for osteoarthritis therapy, *Biomaterials* 295 (2023) 122030, <https://doi.org/10.1016/j.biomaterials.2023.122030>.
- [4] L.B. Yuan, T. Jin, L. Yao, D.H. Yin, Y.Q. Xu, The role and mechanism of biological collagen membranes in repairing cartilage injury through the p38MAPK signaling pathway, *J. Orthop. Surg. Res.* 181 (2023) 837, <https://doi.org/10.1186/s13018-023-04261-y>.
- [5] S.H. Choi, K. Lee, H. Han, H. Mo, H. Jung, Y. Ryu, Y. Nam, Y.A. Rim, J.H. Ju, Prochondrogenic effect of decellularized extracellular matrix secreted from human induced pluripotent stem cell-derived chondrocytes, *Acta Biomater.* 167 (2023) 234–248, <https://doi.org/10.1016/j.actbio.2023.05.052>.
- [6] M. Duan, S. Xia, Y. Liu, X. Pu, Y. Chen, Y. Zhou, M. Huang, C. Pi, D. Zhang, J. Xie, Stiffened fibre-like microenvironment based on patterned equidistant micropillars directs chondrocyte hypertrophy, *Mater Today Bio* 20 (2023) 100682, <https://doi.org/10.1016/j.mtbio.2023.100682>.
- [7] B. Han, W. Fang, Z. Yang, Y. Wang, S. Zhao, B.X. Hoang, C.T. Vangsness Jr., Enhancement of chondrogenic markers by exosomes derived from cultured human synovial fluid-derived cells: a Comparative analysis of 2D and 3D conditions, *Biomedicines* 1112 (2023), <https://doi.org/10.3390/biomedicines11123145>.
- [8] D. Tan, Z. Huang, Z. Zhao, X. Chen, J. Liu, D. Wang, Z. Deng, W. Li, Single-cell sequencing, genetics, and epigenetics reveal mesenchymal stem cell senescence in osteoarthritis (Review), *Int. J. Mol. Med.* 531 (2024), <https://doi.org/10.3892/ijmm.2023.5326>.
- [9] J. Burke, R. Kolhe, M. Hunter, C. Isles, M. Hamrick, S. Fulzele, Stem cell-derived exosomes: a potential alternative therapeutic agent in orthopaedics, *Stem Cell. Int.* 2016 (2016) 5802529, <https://doi.org/10.1155/2016/5802529>.
- [10] H. Hu, L. Dong, Z. Bu, Y. Shen, J. Luo, H. Zhang, S. Zhao, F. Lv, Z. Liu, miR-23a-3p-abundant small extracellular vesicles released from Gelma/nanoclay hydrogel for cartilage regeneration, *J. Extracell. Vesicles* 91 (2020) 1778883, <https://doi.org/10.1080/20013078.2020.1778883>.
- [11] F.-X. Zhang, P. Liu, W. Ding, Q.-B. Meng, D.-H. Su, Q.-C. Zhang, R.-X. Lian, B.-Q. Yu, M.-D. Zhao, J. Dong, Y.-L. Li, L.-B. Jiang, Injectable Mussel-Inspired highly adhesive hydrogel with exosomes for endogenous cell recruitment and cartilage defect regeneration, *Biomaterials* 278 (2021) 121169, <https://doi.org/10.1016/j.biomaterials.2021.121169>.
- [12] J. Huang, J. Xiong, L. Yang, J. Zhang, S. Sun, Y. Liang, Cell-free exosome-laden scaffolds for tissue repair, *Nanoscale* 1319 (2021) 8740–8750, <https://doi.org/10.1039/d1nr01314a>.
- [13] S. Zhang, S.-J. Chuah, R.C. Lai, J.H.P. Hui, S.K. Lim, W.S. Toh, MSC exosomes mediate cartilage repair by enhancing proliferation, attenuating apoptosis and modulating immune reactivity, *Biomaterials* 156 (2018) 16–27, <https://doi.org/10.1016/j.biomaterials.2017.11.028>.
- [14] B.J. Evers, M.H.J. Van Den Bosch, A.B. Blom, P.M. van der Kraan, S. Koeter, R. M. Thurlings, Post-traumatic knee osteoarthritis; the role of inflammation and hemarthrosis on disease progression, *Front. Med.* 9 (2022) 973870, <https://doi.org/10.3389/fmed.2022.973870>.
- [15] Q. Li, H. Yu, F. Zhao, C. Cao, T. Wu, Y. Fan, Y. Ao, X. Hu, 3D printing of microenvironment-specific bioinspired and exosome-reinforced hydrogel scaffolds for efficient cartilage and subchondral bone regeneration, *Adv. Sci.* 1026 (2023) e2303650, <https://doi.org/10.1002/advs.202303650>.
- [16] S. Zhao, G. Xiu, J. Wang, Y. Wen, J. Lu, B. Wu, G. Wang, D. Yang, B. Ling, D. Du, J. Xu, Engineering exosomes derived from subcutaneous fat MSCs specially promote cartilage repair as miR-199a-3p delivery vehicles in Osteoarthritis, *J. Nanobiotechnol.* 211 (2023) 341, <https://doi.org/10.1186/s12951-023-02086-9>.
- [17] E. Chiaradia, B. Tancini, C. Emiliani, F. Delo, R.M. Pellegrino, A. Tognoloni, L. Urbanelli, S. Buratta, Extracellular vesicles under oxidative stress conditions: biological properties and physiological roles, *Cells* 107 (2021), <https://doi.org/10.3390/cells10071763>.
- [18] Y. Jiang, Osteoarthritis year in review 2021: biology, *Osteoarthritis Cartilage* 302 (2022) 207–215, <https://doi.org/10.1016/j.joca.2021.11.009>.
- [19] Y. Pan, S. Cao, A.S. Terker, J. Tang, K. Sasaki, Y. Wang, A. Niu, W. Luo, X. Fan, S. Wang, M.H. Wilson, M.Z. Zhang, R.C. Harris, Myeloid cyclooxygenase-2/prostaglandin E2/E-type prostanoid receptor 4 promotes transcription factor MafB-dependent inflammatory resolution in acute kidney injury, *Kidney Int.* 1011 (2022) 79–91, <https://doi.org/10.1016/j.kint.2021.09.033>.
- [20] H. Li, Y. Yuan, L. Zhang, C. Xu, H. Xu, Z. Chen, Reprogramming macrophage polarization, depleting ROS by astaxanthin and thioketal-containing polymers delivering rapamycin for osteoarthritis treatment, *Adv. Sci.* (2023) e2305363, <https://doi.org/10.1002/advs.202305363>.
- [21] E. Horvath, A. Solyom, J. Szekeley, E.E. Nagy, H. Popoviciu, Inflammatory and metabolic signaling interfaces of the hypertrophic and senescent chondrocyte phenotypes associated with osteoarthritis, *Int. J. Mol. Sci.* 2422 (2023), <https://doi.org/10.3390/ijms242216468>.
- [22] S. Li, D. Niu, H. Fang, Y. Chen, J. Li, K. Zhang, J. Yin, P. Fu, Tissue adhesive, ROS scavenging and injectable PRP-based 'plasticine' for promoting cartilage repair, *Regen Biomater* 11 (2024) rbad104, <https://doi.org/10.1093/rb/rbad104>.
- [23] D. Li, K. Chen, H. Tang, S. Hu, L. Xin, X. Jing, Q. He, S. Wang, J. Song, L. Mei, R. D. Cannon, P. Ji, H. Wang, T. Chen, A logic-based diagnostic and therapeutic hydrogel with multistimuli responsiveness to orchestrate diabetic bone regeneration, *Adv. Mater.* 3411 (2022) 2108430, <https://doi.org/10.1002/adma.202108430>.
- [24] T. Zhou, H. Xiong, S.Q. Wang, H.L. Zhang, W.W. Zheng, Z.R. Gou, C.Y. Fan, C. Y. Gao, An injectable hydrogel dotted with dexamethasone acetate-encapsulated reactive oxygen species-scavenging micelles for combinatorial therapy of osteoarthritis, *Materials Today Nano* 17 (2022) 100164, <https://doi.org/10.1016/j.mtnano.2021.100164>.
- [25] C. Zhao, J. Chen, J. Ye, Z. Li, L. Su, J. Wang, Y. Zhang, J. Chen, H. Yang, J. Shi, J. Song, Structural transformative antioxidants for dual-responsive anti-inflammatory delivery and photoacoustic inflammation imaging, *Angew. Chem. Int. Ed.* 6026 (2021) 14458–14466, <https://doi.org/10.1002/anie.202100873>.
- [26] Y. Liu, Y. Cheng, H. Zhang, M. Zhou, Y. Yu, S. Lin, B. Jiang, X. Zhao, L. Miao, C. W. Wei, Q. Liu, Y.W. Lin, Y. Du, C.J. Butcher, H. Wei, Integrated cascade nanozyme catalyzes in vivo ROS scavenging for anti-inflammatory therapy, *Sci. Adv.* 629 (2020), <https://doi.org/10.1126/sciadv.abb2695>.
- [27] B.R. da Costa, S. Reichenbach, N. Keller, L. Nartey, S. Wandel, P. Juni, S. Trelle, Effectiveness of non-steroidal anti-inflammatory drugs for the treatment of pain in knee and hip osteoarthritis: a network meta-analysis, *Lancet* 39010090 (2017) e21–e33, [https://doi.org/10.1016/S0140-6736\(17\)31744-0](https://doi.org/10.1016/S0140-6736(17)31744-0).
- [28] M. Gao, M. Tang, W. Ho, Y. Teng, Q. Chen, L. Bu, X. Xu, X.Q. Zhang, Modulating plaque inflammation via targeted mRNA nanoparticles for the treatment of atherosclerosis, *ACS Nano* 1718 (2023) 17721–17739, <https://doi.org/10.1021/acsnano.3c00958>.
- [29] M. Wang, Z. Deng, Y. Guo, P. Xu, Designing functional hyaluronic acid-based hydrogels for cartilage tissue engineering, *Mater Today Bio* 17 (2022) 100495, <https://doi.org/10.1016/j.mtbio.2022.100495>.
- [30] K. Lewandowska, Miscibility studies of hyaluronic acid and poly(vinyl alcohol) blends in various solvents, *Materials* 1321 (2020), <https://doi.org/10.3390/ma13214750>.
- [31] Y. Zhu, Y. Matsumura, M. Velayutham, L.M. Foley, T.K. Hitchens, W.R. Wagner, Reactive oxygen species scavenging with a biodegradable, thermally responsive hydrogel compatible with soft tissue injection, *Biomaterials* 177 (2018) 98–112, <https://doi.org/10.1016/j.biomaterials.2018.05.044>.
- [32] S.H. Oh, D.B. An, T.H. Kim, J.H. Lee, Wide-range stiffness gradient PVA/HA hydrogel to investigate stem cell differentiation behavior, *Acta Biomater.* 35 (2016) 23–31, <https://doi.org/10.1016/j.actbio.2016.02.016>.
- [33] H. Hendrawan, H.A. Aziz, N. Haryati, F. Khoerunnisa, Poly(vinyl alcohol)/premnna oblongifolia merr. Extract/glutaraldehyde/carbon nanotube (VOGC)-Based composite hydrogel: a potential candidate for controlled-release materials, *ChemistryOpen* 122 (2023) e202200239, <https://doi.org/10.1002/open.202200239>.
- [34] J. Chen, X. Yang, R. Liu, C. Wen, H. Wang, L. Huang, W. Li, Z. Zhu, Y. Zhu, H. Liu, Circular RNA GLIS2 promotes colorectal cancer cell motility via activation of the NF-kappaB pathway, *Cell Death Dis.* 119 (2020) 788, <https://doi.org/10.1038/s41419-020-02989-7>.
- [35] L. Wang, B. Zhu, Y. Deng, T. Li, Q. Tian, Z. Yuan, L. Ma, C. Cheng, Q. Guo, L. Qiu, Biocatalytic and antioxidant nanostructures for ROS scavenging and biotherapeutics, *Adv. Funct. Mater.* 3131 (2021), <https://doi.org/10.1002/adfm.202101804>.
- [36] C. Antich, J. de Vicente, G. Jimenez, C. Chocarro, E. Carrillo, E. Montanez, P. Galvez-Martin, J.A. Marchal, Bio-inspired hydrogel composed of hyaluronic acid and alginate as a potential bioink for 3D bioprinting of articular cartilage engineering constructs, *Acta Biomater.* 106 (2020) 114–123, <https://doi.org/10.1016/j.actbio.2020.01.046>.
- [37] S.H. Oh, D.B. An, T.H. Kim, J.H. Lee, Wide-range stiffness gradient PVA/HA hydrogel to investigate stem cell differentiation behavior, *Acta Biomater.* 35 (2016) 23–31, <https://doi.org/10.1016/j.actbio.2016.02.016>.
- [38] S. Meng, H. Hu, Y. Qiao, F. Wang, B.N. Zhang, D. Sun, L. Zhou, L. Zhao, L. Xie, H. Zhang, Q. Zhou, A versatile hydrogel with antibacterial and sequential drug-releasing capability for the programmable healing of infectious keratitis, *ACS Nano* 1723 (2023) 24055–24069, <https://doi.org/10.1021/acsnano.3c09034>.
- [39] Y. Zhan, W. Fu, Y. Xing, X. Ma, C. Chen, Advances in versatile anti-swelling polymer hydrogels, *Mater. Sci. Eng. C* 127 (2021) 112208, <https://doi.org/10.1016/j.msec.2021.112208>.
- [40] D. Sivaraj, K. Chen, A. Chattopadhyay, D. Henn, W. Wu, C. Noishiki, N.J. Magbual, S. Mittal, A.M. Mermin-Bunnell, C.A. Bonham, A.A. Trotsyuk, J.A. Barrera, J. Padmanabhan, M. Januszky, G.C. Gurtner, Hydrogel scaffolds to deliver cell therapies for wound healing, *Front. Bieng. Biotechnol.* 9 (2021) 660145, <https://doi.org/10.3389/fbioe.2021.660145>.
- [41] M. Assuncao, C.H.K. Yiu, H.Y. Wan, D. Wang, D.F.E. Ker, R.S. Tuan, A. Blocki, Hyaluronic acid drives mesenchymal stromal cell-derived extracellular matrix assembly by promoting fibronectin fibrillogenesis, *J. Mater. Chem. B* 935 (2021) 7205–7215, <https://doi.org/10.1039/d1tb00268f>.

- [42] M. Daheshia, J.Q. Yao, The interleukin 1 β pathway in the pathogenesis of osteoarthritis, *J. Rheumatol.* 3512 (2008) 2306–2312, <https://doi.org/10.3899/jrheum.080346>.
- [43] R. Mata, Y. Yao, W. Cao, J. Ding, T. Zhou, Z. Zhai, C. Gao, The Dynamic Inflammatory Tissue Microenvironment: Signality and Disease Therapy by Biomaterials, 2021, Research (Wash D C), 2021 4189516, <https://doi.org/10.34133/2021/4189516>.
- [44] J. Chen, J. Yang, L. Wang, X. Zhang, B.C. Heng, D.-A. Wang, Z. Ge, Modified hyaluronic acid hydrogels with chemical groups that facilitate adhesion to host tissues enhance cartilage regeneration, *Bioact. Mater.* 66 (2020) 1689–1698, <https://doi.org/10.1016/j.bioactmat.2020.11.020>.
- [45] V. Deshmukh, A.L. O'Green, C. Bossard, T. Seo, L. Lamangan, M. Ibanez, A. Ghias, C. Lai, L. Do, S. Cho, J. Cahiwat, K. Chiu, M. Pedraza, S. Anderson, R. Harris, L. Dellamary, S. Kc, C. Barroga, B. Melchior, B. Tam, S. Kennedy, J. Tambiah, J. Hood, Y. Yazici, Modulation of the Wnt pathway through inhibition of CLK2 and DYRK1A by lorecivint as a novel, potentially disease-modifying approach for knee osteoarthritis treatment, *Osteoarthritis Cartilage* 279 (2019) 1347–1360, <https://doi.org/10.1016/j.joca.2019.05.006>.
- [46] M. Coma, L. Frohlichova, L. Urban, R. Zajicek, T. Urban, P. Szabo, S. Novak, V. Fetisov, B. Dvorankova, K. Smetana Jr., P. Gal, Molecular changes underlying hypertrophic scarring following burns involve specific deregulations at all wound healing stages (inflammation, proliferation and maturation), *Int. J. Mol. Sci.* 222 (2021), <https://doi.org/10.3390/ijms22020897>.
- [47] M.L. Vainieri, A. Lolli, N. Kops, D. D'Atri, D. Eglin, A. Yayon, M. Alini, S. Grad, K. Sivasubramanian, G. van Osch, Evaluation of biomimetic hyaluronic-based hydrogels with enhanced endogenous cell recruitment and cartilage matrix formation, *Acta Biomater.* 101 (2020) 293–303, <https://doi.org/10.1016/j.actbio.2019.11.015>.
- [48] K.P. McCreery, C.M. Luetkemeyer, S. Calve, C.P. Neu, Hyperelastic characterization reveals proteoglycans drive the nanoscale strain-stiffening response in hyaline cartilage, *J. Biomech.* 146 (2023) 111397, <https://doi.org/10.1016/j.jbiomech.2022.111397>.
- [49] T.A. Wynn, K.M. Vannella, Macrophages in tissue repair, regeneration, and fibrosis, *Immunity* 443 (2016) 450–462, <https://doi.org/10.1016/j.immuni.2016.02.015>.
- [50] C.L. Hawkins, M.J. Davies, Role of myeloperoxidase and oxidant formation in the extracellular environment in inflammation-induced tissue damage, *Free Radic. Biol. Med.* 172 (2021) 633–651, <https://doi.org/10.1016/j.freeradbiomed.2021.07.007>.
- [51] X. Hu, B. Li, F. Wu, X. Liu, M. Liu, C. Wang, Y. Shi, L. Ye, GPX7 facilitates BMSCs osteoblastogenesis via ER stress and mTOR pathway, *J. Cell Mol. Med.* 2522 (2021) 10454–10465, <https://doi.org/10.1111/jcmm.16974>.
- [52] Q. Chen, C. Che, S. Yang, P. Ding, M. Si, G. Yang, Anti-inflammatory effects of extracellular vesicles from *Morchella* on LPS-stimulated RAW264.7 cells via the ROS-mediated p38 MAPK signaling pathway, *Mol. Cell. Biochem.* 4782 (2023) 317–327, <https://doi.org/10.1007/s11010-022-04508-y>.
- [53] Q. Wei, N. Kong, X. Liu, R. Tian, M. Jiao, Y. Li, H. Guan, K. Wang, P. Yang, Pirfenidone attenuates synovial fibrosis and postpones the progression of osteoarthritis by anti-fibrotic and anti-inflammatory properties in vivo and in vitro, *J. Transl. Med.* 191 (2021) 157, <https://doi.org/10.1186/s12967-021-02823-4>.
- [54] J. Zhang, J. Zhou, Q. Yuan, C. Zhan, Z. Shang, Q. Gu, J. Zhang, G. Fu, W. Hu, Characterization of ginsenoside compound K loaded ionically cross-linked carboxymethyl chitosan-calcium nanoparticles and its cytotoxic potential against prostate cancer cells, *J. Ginseng Res* 452 (2021) 228–235, <https://doi.org/10.1016/j.jjgr.2020.01.007>.
- [55] H.P. Lee, F. Alisafaei, K. Adebawale, J. Chang, V.B. Shenoy, O. Chaudhuri, The nuclear piston activates mechanosensitive ion channels to generate cell migration paths in confining microenvironments, *Sci. Adv.* 72 (2021), <https://doi.org/10.1126/sciadv.abd4058>.
- [56] A.K. Gill, P.J. McCormick, D. Sochart, G. Nalesso, Wnt signalling in the articular cartilage: a matter of balance, *Int. J. Exp. Pathol.* 1042 (2023) 56–63, <https://doi.org/10.1111/iep.12472>.
- [57] N. Fahy, E. Farrell, T. Ritter, A.E. Ryan, J.M. Murphy, Immune modulation to improve tissue engineering outcomes for cartilage repair in the osteoarthritic joint, *Tissue Eng., Part B* 211 (2015) 55–66, <https://doi.org/10.1089/ten.TEB.2014.0098>.